

Review

Abatement of VOCs Using Packed Bed Non-Thermal Plasma Reactors: A Review

Savita K. P. Veerapandian *, Christophe Leys, Nathalie De Geyter and Rino Morent

Department of Applied Physics, Research Unit Plasma Technology, Faculty of Engineering and Architecture, Ghent University, Sint-Pietersnieuwstraat 41, 9000 Ghent, Belgium; Christophe.leys@ugent.be (C.L.); Nathalie.DeGeyter@UGent.be (N.D.G.); Rino.morent@ugent.be (R.M.)

* Correspondence: Savita.kaliyaperumalveerapandian@ugent.be; Tel.: +32-9-264-3838

Academic Editor: Jean-François Lamonier

Received: 20 December 2016; Accepted: 7 April 2017; Published: 12 April 2017

Abstract: Non thermal plasma (NTP) reactors packed with non-catalytic or catalytic packing material have been widely used for the abatement of volatile organic compounds such as toluene, benzene, etc. Packed bed reactors are single stage reactors where the packing material is placed directly in the plasma discharge region. The presence of packing material can alter the physical (such as discharge characteristics, power consumption, etc.) and chemical characteristics (oxidation and destruction pathway, formation of by-products, etc.) of the reactor. Thus, packed bed reactors can overcome the disadvantages of NTP reactors for abatement of volatile organic compounds (VOCs) such as lower energy efficiency and formation of unwanted toxic by-products. This paper aims at reviewing the effect of different packing materials on the abatement of different aliphatic, aromatic and chlorinated volatile organic compounds.

Keywords: abatement of VOC; packed bed reactors; non-thermal plasma

1. Introduction

Abatement of low concentration of volatile organic compounds (VOCs) from air is of great interest in the past two decades for environmental remediation. VOCs are organic compounds with very high vapor pressure, which are found in trace amounts in the atmosphere (typically less than 1000 ppm). Emission of VOCs into the atmosphere is of great concern due to its adverse effect on humans (carcinogen, affects central nervous system (CNS), causes respiratory problem, etc.) and the environment (ozone depletion, photochemical smog, global warming, etc.). The sources and the adverse effects of different VOCs on human and environment are shown in Table 1.

Conventional techniques like adsorption [1], absorption [2,3], condensation [4,5], catalytic oxidation [6,7], photocatalysis [8–10], membrane purification [11] and biological treatment [12,13] which have been used for removal of VOCs have disadvantages such as low efficiency and high energy consumption. The merits and demerits of various technologies available for the abatement of VOCs are reviewed in the work by Khan et al. [14], Parmar et al. [15] and Luengas et al. [16]. For example, in catalytic oxidation, the catalyst has to be heated and maintained at higher temperature throughout the process [17]. In thermal oxidation, large amount of energy is used to heat the large volume of gas containing very low concentration of VOCs [18]. Thus, the above mentioned techniques are not cost effective to treat the waste gas when the concentration of VOC is less than 1000 ppm, as it is difficult to maintain the adiabatic conditions [19]. Alternatively, non-thermal plasma (NTP) technology is cost effective in converting diluted VOCs in large volume of air into less toxic substances [20–23]. NTP technology utilizes the supplied energy to create high energy electrons whose temperature is in the range of 10,000–250,000 K (1–25 eV) [24]; whereas the temperature of other particles remains close to room temperature [25,26]. Thus, the electrons are not in thermal equilibrium with other particles

and the overall temperature of the system is maintained close to room temperature. These energetic electrons collide with carrier gas molecules, which is predominantly air and generate highly reactive species such as ground and excited atomic oxygen and nitrogen, and vibrationally and electronically excited oxygen and nitrogen molecules. These reactive species in turn oxidize the diluted VOCs into less toxic substances such as H₂O, CO₂ and other by-products.

Although different types of NTP discharge at atmospheric pressure and room temperature such as corona discharge [27–30], surface discharge (SD) [31], microwave discharge [32], dielectric barrier discharge (DBD) [33–37], packed bed DBD (PBDBD) [38–40] have been widely investigated as an alternative technology to remove VOCs from exhaust gas, formation of unwanted by-products and high energy consumption are the main bottlenecks for the commercialization of the technology. For the development of better NTP technology for abatement of VOCs, the two important factors to be considered in addition to decomposition efficiency are (i) reducing energy consumption and (ii) controlling the formation of unwanted and toxic by-products such as newly formed other VOCs, ozone, NO_x, SO_x [41]. It has been widely reported in the literature that DBD reactors packed with non-catalytic or catalytic materials enhance the energy efficiency [20,42] and reduce the formation of unwanted by-products by total oxidation of aliphatic (methane, butane, ethylene, formaldehyde, acetaldehyde, acetone, bromomethane), aromatic (benzene, toluene, styrene, xylene, chlorobenzene) and halogenated (carbon tetrachloride, dichloromethane, perfluoroethane) VOCs. The effect of different packing materials on the discharge characteristics of the reactor, decomposition efficiency of different VOCs and formation of by-products are summarized in Table 2.

The presence of packing material in the discharge region of the reactor enhances the electric field near the contact points between the dielectric pellets and increases the residence time of VOCs in the discharge region resulting in enhanced removal efficiency [43] and deep oxidation [44] of VOCs respectively. The total oxidation of VOCs in packed bed reactors depends on the properties of packing materials (dielectric constant, size, shape, surface properties and catalytic activity), presence of humidity, energy density and nature of VOC itself. For example, aromatic compound with side chain requires lower energy for complete oxidation when compared to the aromatic compound without sidechain like benzene [45]. This is because the ionization potential of benzene is higher than aromatic compounds with sidechain like xylene or toluene [46].

In this review, the overview of the literature on the packed bed dielectric barrier discharge (PBDBD) reactors for the abatement of different volatile organic compounds is presented. In the first part, different types of packed bed reactors which have been used for VOC removal are reviewed. In the second part, the influence of different properties of the packing materials such as dielectric constant, packing material shape and size, surface properties (porosity and surface area) on the performance of packed bed reactors for the decomposition of different VOCs are reported. The effect of addition of catalysts or catalytic packing material on decomposition efficiency (η), carbon balance (the ratio between the carbon converted from VOC to gaseous by-products and the total carbon converted in the process), CO₂ selectivity (the ratio between the carbon converted from VOC to CO₂ and the total carbon converted in the process) and by-product formation is also reviewed.

2. Packed Bed Reactors

Packed bed reactors are single stage reactors in which a non-catalytic/catalytic packing material is located in the discharge region of the reactor. The schematic of the most commonly used configuration of packed bed reactors are shown in Figure 1. The PBDBD reactors used for the abatement of VOCs consist of a discharge (high voltage) electrode and a ground electrode separated by one or two dielectric layers and the space between the dielectric layer and one of the electrode is filled with the packing material. Quartz or glass tubes are widely used as dielectric barrier in the packed bed reactors used for the decomposition of VOCs.

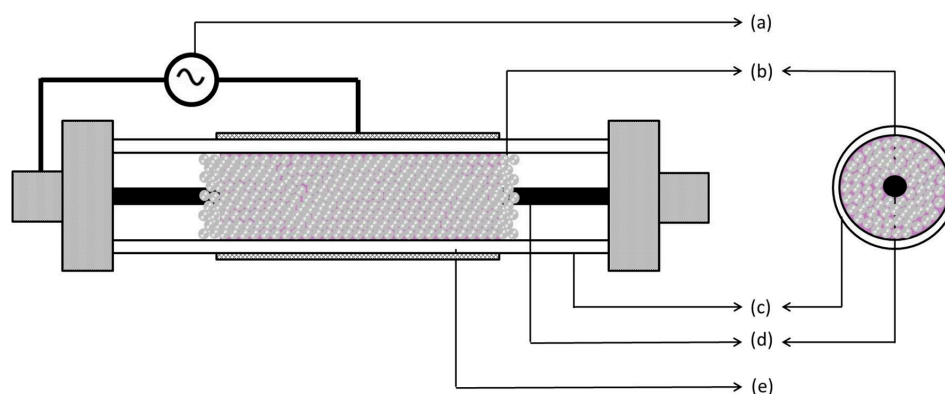


Figure 1. Schematic diagram of packed bed non-thermal plasma reactor and its cross-sectional view (a) Power source; (b) Packing material in discharge gap; (c) Dielectric barrier; (d) High voltage (or powered electrode) and (e) Ground electrode.

The high voltage (or discharge) electrode can be made of stainless steel rod [47–51], stainless steel wire [52,53], stainless steel spring [54,55], stainless steel bolt [56,57], aluminum rod [58], copper rod [59], molybdenum rod [60] or tungsten wire [43,61–63]. The surface area and geometry of the inner electrode plays an important role in the discharge characteristics of the plasma reactor. For example, increasing the diameter of the inner electrode, reduces the discharge gap and increases the superficial area resulting in a uniform distribution of microdischarges and a higher number of energetic secondary electrons [61] respectively. The geometry of the electrode affects the number of microdischarges per cycle of applied voltage [64]. Using a bolt instead of a wire or rod as high voltage electrode enhances electric field at the sharp edges of the bolt and increases the number of microdischarges resulting in higher removal and power efficiency [37,56,65]. In PBDBD reactors, the length of the ground electrode determines the effective length of the reactor. The ground electrode can be made of aluminum tape [47,52,55], copper mesh [52,58,63,66], stainless steel mesh [43,56,60], iron mesh [61], aluminum mesh [50], silver paste [51,52], stainless steel foil [53], brass wire [62] or aluminum foil [59,67,68]. Using metal wire, tape or gauze as ground electrode can form void between ground electrode and dielectric barrier which results in a corona discharge in the void. The energy consumed by the corona discharge in the void does not contribute to the decomposition of VOC and results in increased energy consumption and decreased conversion efficiency. In literature, it has been mentioned that painting silver paste on the wall of the discharge tube [41,52,69] prevents the formation of voids and improves the conductivity between electrode.

The DBD reactor with packing material operates with a small volume fraction of plasma when compared to the unpacked reactor [70] and this packing material can be non-catalytic or catalytic. The most commonly used packing materials for the abatement of VOCs are (i) non catalytic materials such as glass, Al_2O_3 , TiO_2 , MnO_2 , activated carbon, graphene oxide (GO), Raschig ring (RR), Zeolites (HZSM-5, ferrierite, H-Y), glass wool (GW), molecular sieve (MS-3A, MS-4A, MS-5A, MS-13X, OMS-2), ferroelectric materials like BaTiO_3 , NaN_2 , SrTiO_3 , CaTiO_3 , Mg_2TiO_4 and (ii) catalytic materials such as metal oxides and noble metal loaded metal oxides.

In PBDBD reactors, when high voltage is applied across the dielectric barrier, the dielectric packing material is polarized which enhances the electric field around the contact points resulting in a partial discharge [71,72]. As shown in Figure 2, the presence of packing materials in the discharge region maximizes the number of micro streamers and thus producing more high energy electrons [18]. These energetic electrons produce reactive intermediates resulting in increased VOC removal efficiency when compared to the unpacked reactors [57,73,74]. Surface discharges produced along the surface of the packing material may distribute the plasma more evenly and intensively throughout the reactor [75] and the catalytic reactions occur on the surface of the packing material. Thus, the use of packed bed reactor gives the advantage of uniform distribution of gas flow and discharge [76]. In packed bed

reactors, absorbents are also used as packing material which increase the residence time and minimize the volume of free gas in the discharge region [77] resulting in increased collisional probability between VOC and active species.

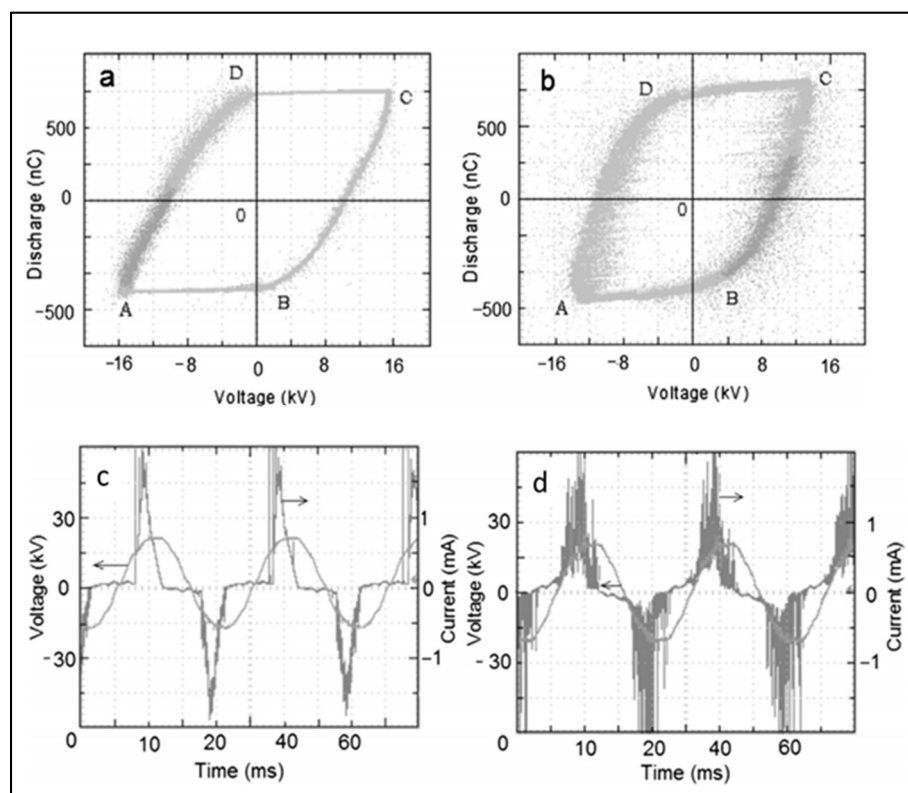


Figure 2. V-Q Lissajous figure in the (a) absence and (b) presence of ceramic Raschig rings (RR), voltage and current waveform in the (c) absence and (d) presence of ceramic Raschig rings (RR) at applied voltage of 12 kV (50 Hz and sine wave). Reprinted from [63]. Copyright (2016), with permission from Elsevier.

The presence of packing material enhances the energy efficiency of the NTP reactor. The presence of packing material in the discharge region reduces the breakdown voltage required for ignition of plasma by enhancing the electric field near the contact points. As shown in Figure 3, the power consumption of the packed reactors are smaller when compared to the unpacked reactor [78] under the same operational conditions. The presence of the packing material in the reactor can reduce the output power and output current [79] for the same applied voltage due to the higher space charge effect. However the average power density (=input power/gas space) of the packed reactor is higher than the unpacked reactor as the volume of the plasma zone in the packed reactor is smaller than the unpacked one. The performance of the non-packed and packed reactors can also be compared using the energy effectiveness (=g VOC removed/kWh). In [79], Lin et al. showed that the energy effectiveness of a glass beads packed bed reactor is 1.5 times higher when compared to the unpacked reactor. The specific energy density required for the non-packed reactor is quite higher than the packed reactor to obtain similar decomposition efficiency [80].

The different kinds of power source used to provide energy for the packed bed plasma reactor are alternating current (ac) or bipolar pulsed power sources [54]. Although a bipolar pulsed power source is expensive, it has advantages over ac power source such as instantaneous energy input [54] and can avoid the accumulation of net charges on the surface of dielectrics [54]. In [81], Duan et al. compared the traditional ac power supply of 50 Hz and bipolar pulse power supply of 50 Hz (peak-to-peak voltage $V_{pp} = 0$ to 30 kV; pulse width 100 ns and pulse rise rate $500 \text{ V} \cdot (\text{ns})^{-1}$). In this work, it is

shown that the discharge current produced by bipolar pulsed power supply is higher and longer when compared to ac power supply with same frequency and applied voltage [81] and the bipolar pulsed power can enhance the chlorobenzene removal efficiency by 1.6 times when compared to ac power supply. However, for economic reason, ac power supply is widely used.

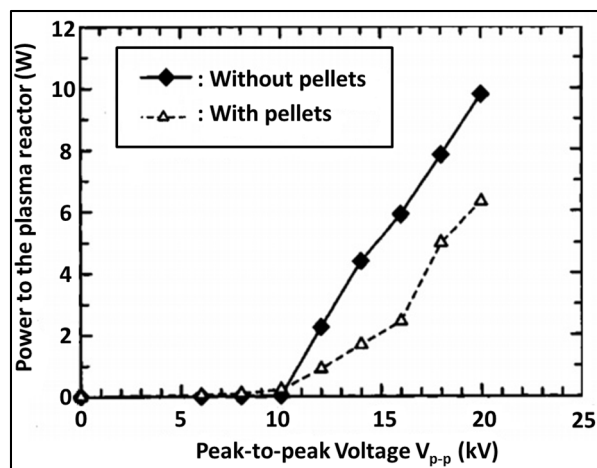


Figure 3. Effect of presence of packing material on the power to the plasma reactor (frequency of power supply = 60 Hz; packing material: BaTiO₃ pellets). Reprinted from [78]. Copyright (2016), with permission from IEEE.

The power consumed by packed bed reactors for the discharge can be calculated using Lissajous curve [25] or by integrating the current and voltage waveform over one period [82,83]. In Lissajous method, the voltage applied on the high voltage electrode is measured using a high voltage probe and the dissipated charge is measured across a capacitor of capacitance C_m , which is connected in series with the ground electrode. The energy deposited in the plasma reactor per cycle is calculated from the area S of the V-Q Lissajous (Figure 2a,b) diagram which has been recorded using a digital oscilloscope. The average power P during discharge is calculated by multiplying the energy deposited per cycle by ac power frequency f [84],

$$P = Sf \quad (1)$$

In the second method, the average power, P , of the discharge is calculated using following equation from the measurement of the current and the voltage over one cycle.

$$P = \frac{1}{T} \int_t^{t+T} I(t)V(t)dt \quad (2)$$

where $V(t)$ and $I(t)$ are instantaneous voltage and current. The discharge current, I , is measured through a resistor in series with the grounded electrode. The applied voltage $V(t)$, and the current variations $I(t)$ with time are visualized using a digital oscilloscope. The specific input energy (SIE) which is widely used in literature to study the energy efficiency of the process and reactor in abatement of VOC is defined as the energy deposited in the flue gas per unit volume and it is given by [85]:

$$SIE (J/L) = \frac{P (W)}{\text{Flow rate (L/s)}} \quad (3)$$

The frequency of the ac power supply also influences the energy efficiency of the DBD reactor. Ogata et al. [66,86] reported that the conversion of benzene decreases with increase in ac frequency applied to the DBD reactor. In [65], it has been reported that the energy efficiency for trichloroethylene (TCE) removal is higher with a 50 Hz ac power supply when compared to higher frequencies such as

500 and 2000 Hz. This decrease in energy efficiency at higher frequency is mainly due to the significant convection [87] (thermal transfer between plasma and dielectric surface) and displacement [87] (the current generated by charging the capacitance of the DBD reactor) current which are not useful for the decomposition of the chemical compounds.

3. Properties of Packing Material

3.1. Dielectric Constant

When an electric field is applied across a dielectric material, the factor by which the effective electric field is reduced by polarization of the dielectric material itself is the dielectric constant. The dielectric constant of a packing material determines the amount of energy the reactor can store during a single discharge [88]. When the applied ac voltage is beyond the breakdown voltage of the interstitial space between packing material, a discharge plasma is formed. The electric field in these interstitial space is amplified by the presence of packing material near the contact points [22] of the packing material and the electric field is higher for the pellets of higher dielectric constant due to boundary conditions of electric flux [89]. The applied voltage and discharge current waveforms for BaTiO₃ pellets of different dielectric constant ($\epsilon_s = 10,000$, 5000 and 660) are shown in Figure 4. The discharge current increases with increase in the dielectric constant of the pellet and it is maximum for the pellet of dielectric constant 10^4 .

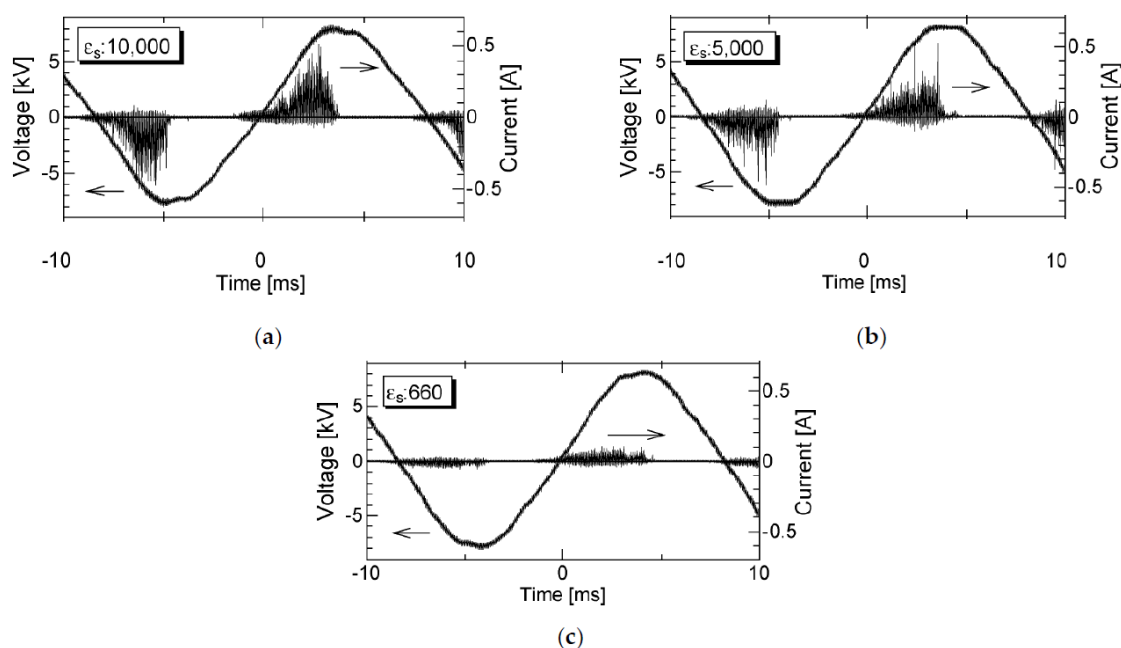


Figure 4. Waveforms of applied voltage and discharge current for different dielectric constant of spherical pellets (a) 10^4 ; (b) 5000 and (c) 650 (applied voltage = 14 kV; frequency = 60 Hz). Reprinted from [90]. Copyright (2016), with permission from IEEE.

Packing material with a higher dielectric constant decreases the breakdown voltage [91] and enhances the electric field resulting in enhanced VOC removal efficiency [92]. Zheng et al. [88] pointed out that the packing material with higher dielectric constant (γ -Al₂O₃) enhances the removal efficiency of acetone when compared to glass beads. When an external ac voltage beyond onset voltage is applied across a dielectric barrier with higher dielectric constant, an intense electric field is produced in the area near the contact point of the pellets and results in a combination of surface discharges on the packing pellets and filamentary discharges in the voids [43,93]. As shown in Figure 5, ferroelectric packing materials with dielectric constant $\epsilon_r \geq 1100$ are energy efficient in benzene removal (amount of benzene

removed per watt) [86]. In [61], Liang et al. reported that the BaTiO₃ packed bed reactor has the highest toluene removal efficiency when compared to a NaNO₂ PBDBD reactor, as the spontaneous polarization intensity of BaTiO₃ is higher than NaNO₂. Thus, the usage of ferroelectric pellets enhances the electric field (by a factor of 10–250) by polarization [72], resulting in the formation of higher-energetic species in the discharge zone [94] and thus an enhanced VOC removal efficiency.

Apart from VOC removal efficiency, the dielectric constant of the packing material also plays an important role in the formation of by-products such as ozone, NO_x. According to Futamura et al. [41], the nature of the catalyst or the packing material has less effect on the initial conversion of VOC. However, it has more influence on the reaction of intermediates formed leading to a difference in the carbon balance and CO₂ selectivity. Ogata et al. [86] reported that the ferroelectric packing material with lower dielectric constant suppresses the formation of NO_x, but produces large amount of ozone. Coating dielectric material with metals of higher conductivity reduces the polarization of the pellets and thus the decomposition efficiency. In [71], it is reported that BaTiO₃ pellets showed better removal efficiency when compared to 0.2 wt % Pt coated BaTiO₃ due to the increased conductivity of the pellets by platinum coating. The dielectric constant of the material varies as a function of temperature. For example, the dielectric constant of the ferroelectric packing material Urashima et al. [92] reported that the temperature of the DBD reactor and thus the packing material increases during the operation, resulting in a reduced dielectric constant of the ferroelectric packing material. Thus, the electric field in the vicinity of the pellets is reduced resulting in reduced VOC removal efficiency.

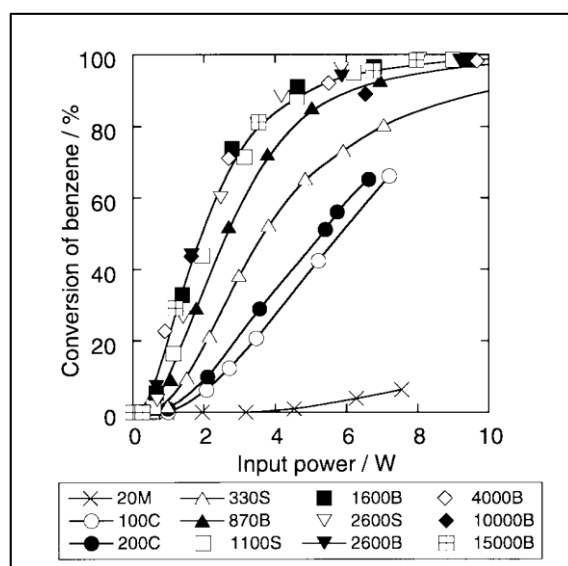


Figure 5. Effect of dielectric constant on the removal efficiency of benzene (Initial benzene concentration: 200 ppm; carrier gas: dry air; flow rate: 0.2 L/min; shape and size of the packing material: sphere of ϕ 2 mm, numbers in legend box refer to dielectric constant value, M = Mg₂TiO₄, C = CaTiO₃, S = SrTiO₃, B = BaTiO₃). Reprinted from [86]. Copyright (2016), with permission from IEEE.

3.2. Packing Material Size

The size of the packing materials plays an important role in determining the characteristics of discharges in the reactor and the efficiency of VOC decomposition. The diameter of the packing material is chosen to maximize the contact points between the packing materials of same size without completely filling the discharge gap. Ogata et al. [86,95] mentioned that BaTiO₃ pellets of larger diameter (3 mm) are less efficient in decomposing benzene when compared to the smaller pellets. Similarly, Yamamoto et al. [38] mentioned that much higher toluene decomposition efficiency is obtained by using BaTiO₃ pellets of smaller diameter. In [71], it is reported that BaTiO₃ pellets of

smaller diameter (1 mm) are more efficient in removing CCl_4 when compared to pellets of diameter 3 mm. This is attributed to the enhanced electric field and more uniform plasma throughout the reactor volume when packed with smaller pellets. Contrarily, it has been reported in [96] that very fine titania pellets (~0.5 to 1 mm) reduced the removal efficiency of TCE. This is due to the insufficient generation of plasma in the reactive region as there is lack of void due to the compact packing of titania.

3.3. Packing Material Shape

Packing material made of the same material but with different shape can influence the capacitance of the reactor which changes the discharge characteristics [97] and thus VOC removal efficiency [79]. The waveforms of applied voltage and discharge current for various pellet shapes such as (a) sphere, (b) solid cylinder and (c) hollow cylinder are shown in Figure 6. The discharge current waveforms of the three different packing shapes show that the formation of microdischarges follows the following sequence: hollow cylinder > cylinder > sphere. Takaki et al. [90] showed that for the same applied voltage, the quantity of charge accumulated with the microdischarge current in a hollow cylindrical pellet is higher when compared to spherical and cylindrical pellet. The micro-discharges start appearing at lower voltage for the hollow cylinder. This is because the enhancement of electric field is higher for the hollow cylinder due to the presence of sharp edges [98]. The DBD reactor filled with hollow cylindrical pellet showed higher energy efficiency (g/kWh) in the abatement of C_2F_6 when compared with spherical pellets. In [96], Oda et al. showed that the removal efficiency showed by disc shaped randomly crushed TiO_2 is higher when compared to spherical ones. This is due to the presence of sharp edges in the packing material which enhances the electric field.

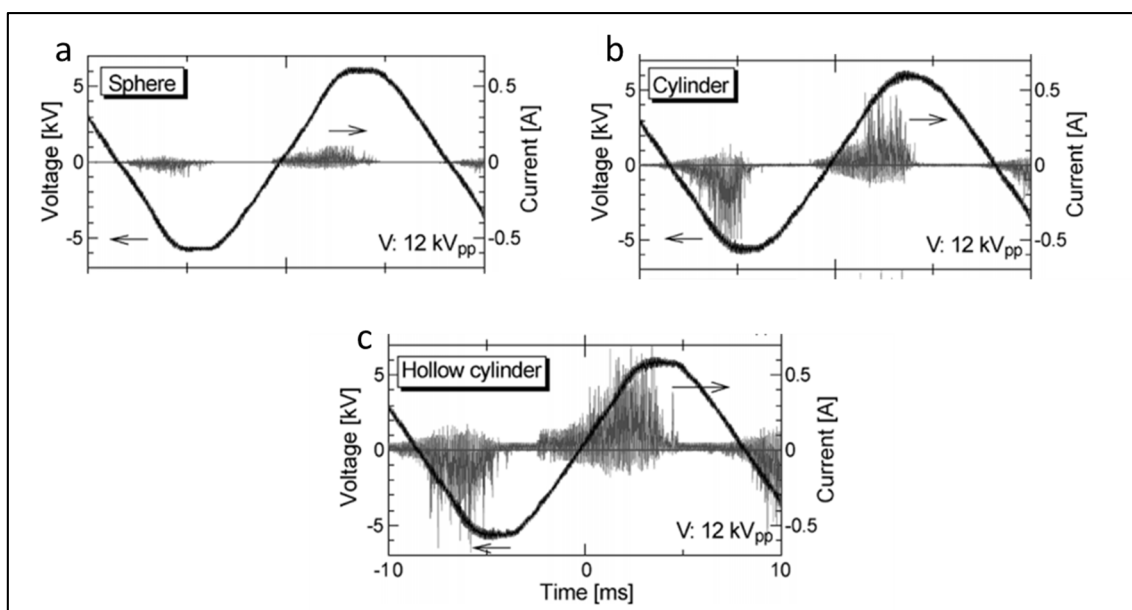


Figure 6. Waveforms of applied voltage and discharge current for different pellet shape such as (a) sphere; (b) cylinder and (c) hollow cylinder (packing material = BaTiO_3 ; dielectric constant = 10^4 ; applied voltage = 12 kV; frequency = 60 Hz). Reprinted from [90]. Copyright (2016), with permission from IEEE.

3.4. Surface Properties

The surface properties of the packing material such as surface area, pore volume and pore size play an important role in complete oxidation of VOCs. These properties of the packing material affect the residence time of the VOCs in the discharge region of the reactor by adsorption and increases the collision probability between adsorbed pollutant molecules and the plasma generated active species.

As the adsorbed molecules can only vibrate at their fixed position, they can be more easily attacked by the reactive species when compared to the randomly moving gas phase molecules. For example, adsorption packing materials such as Al_2O_3 and zeolites concentrate VOCs on their surface resulting in enhanced collisional probability and deep oxidation of VOCs. Adsorption lowers the bond energy of the VOC molecule [88] and weakens the chemical bond which enhances the dissociation when these adsorbed molecules encounters the active species in the plasma [99]. The most commonly used porous packing materials in DBD reactor for the abatement of VOCs are porous alumina, activated carbon and zeolites.

Lee et al. [100] reported that a reactor packed with porous $\gamma\text{-Al}_2\text{O}_3$ results in complete oxidation of benzene and enhanced CO_2 selectivity due to an increase in residence time. Liang et al. [43] reported that Al_2O_3 increases the residence time of toluene in the reactor resulting in enhanced toluene removal rate. This is because porous alumina possess electron-accepting acidic center which acts as an adsorption material for compound with π -electrons [101]. He et al. [73] reported that the activated carbon exhibits higher removal efficiency of benzene due to its higher surface area ($S_{\text{BET}} = 609.3 \text{ m}^2/\text{g}$) when compared to other packing materials such as alumina ($S_{\text{BET}} = 230 \text{ m}^2/\text{g}$) and molecular sieve ($S_{\text{BET}} = 45 \text{ m}^2/\text{g}$).

In literature, it has been reported that packing the reactor with the same material but different surface properties like surface area and porosity influences the oxidation of VOCs and formation of by-products. Gandhi et al. [102], reported that the ethylene decomposition efficiency is enhanced with porous alumina ($S_{\text{BET}} = 348.3 \text{ m}^2/\text{g}$) when compared to non-porous alumina ($S_{\text{BET}} = 1.53 \text{ m}^2/\text{g}$). Also the complete oxidation of ethylene to CO_2 and CO is obtained with porous alumina, whereas non-porous alumina leads to the formation of by-products such as acetaldehyde, acetylene and methane in addition to CO and CO_2 . Ogata et al. [95] found that CO_2 selectivity has been enhanced with a DBD reactor packed with porous Al_2O_3 when compared to non-porous Al_2O_3 due to complete oxidation of benzene in the adsorbed phase. Zheng et al. [88] reported that alumina with higher surface area ($\gamma\text{-Al}_2\text{O}_3$, $S_{\text{BET}} = 174 \text{ m}^2/\text{g}$) shows better acetone removal due to adsorption when compared to the $\alpha\text{-Al}_2\text{O}_3$ ($S_{\text{BET}} = 53 \text{ m}^2/\text{g}$). In [42], it has been reported that the removal efficiency of formaldehyde (HCHO) with $\gamma\text{-Al}_2\text{O}_3$ ($S_{\text{BET}} \approx 220 \text{ m}^2/\text{g}$) is higher when compared to $\alpha\text{-Al}_2\text{O}_3$ ($S_{\text{BET}} \approx 10 \text{ m}^2/\text{g}$) due to the difference in the specific surface area. Adsorption of HCHO reduces the dissociation threshold energy. Ogata et al. [44] reported that the energy efficiency of a $\text{Al}_2\text{O}_3/\text{BaTiO}_3$ packed bed reactor is enhanced when compared to a BaTiO_3 packed reactor. This finding shows that in addition to decomposition of benzene in the gas phase on the surface of BaTiO_3 , there is also the disappearance of benzene due to adsorption on porous Al_2O_3 . In [96], it has been reported that titania pellets with higher surface area showed an enhanced removal efficiency of TCE. Pangilinan et al. [49] showed that silver loaded TiO_2 with lower surface area ($S_{\text{BET}} = 49 \text{ m}^2/\text{g}$) decomposes benzene up to 20%; whereas the Ag/TiO_2 with higher surface area ($S_{\text{BET}} \approx 63 \text{ m}^2/\text{g}$) completely oxidizes benzene. The increase in surface area enhances the adsorption of benzene on a catalytic surface results in enhanced decomposition. In [18], Cu–Ce catalyst showed both a better removal efficiency of HCHO and a better CO_2 selectivity when compared to CuO or CeO_2 . This is because the specific surface area and the pore volume of the Cu–Ce catalyst is larger when compared to the other catalysts which promotes the adsorption of VOCs and increases the retention time of the pollutant in the discharge region and enhances the deep oxidation [103].

Hu et al. [54] and Ogata et al. [104] reported that CO_2 selectivity is greatly enhanced by zeolite hybrid reactors due to the porous structure of zeolites which increases the residence time of the adsorbed species resulting in an increased collisional probability between VOC and active species. The external surface area of zeolites is much smaller when compared to the total surface area (which includes micro and macro-pores). However the results suggest that benzene adsorbed on the external pores are readily oxidized when compared to the ones adsorbed on the internal pores [104]. The higher surface area and pore volume of HZSM-5 packing material enhance the adsorption of chlorobenzene and residence time and results in a higher removal efficiency and a good

CO₂ selectivity [105]. In [65], it has been reported that the presence of V₂O₅/TiO₂ or Cu-ZSM-5 enhances the decomposition of TCE partly due to the adsorption of TCE on the packing material.

The porous packing material adsorbs/adsorbs molecules of sizes smaller than its pore size [106]. When the pore size of a packing material is larger than the size of the VOC molecule, there is an increased probability of VOC adsorption in these micro-pores. In [41], benzene decomposition is studied using two types of zeolite, H-Y and ferrierite, with pore diameter 7.4 Å and 4.3–5.3 Å respectively. It is shown that benzene (molecular size = 5.9 Å) can assimilate well in the micro-pores of H-Y when compared to ferrierite. This is because the pore size of H-Y is bigger than the molecular size of benzene.

Packing the DBD reactor with porous material (Al₂O₃ and SiO₂) enhances the discharge power when compared to non-porous (ZrO₂ and GW) packing material. This is due to the formation of micro-discharges in the micro-pores in addition to the micro-discharges in the gas phase [107]. In addition to the enhanced discharge power, the adsorption of ethylene in these porous material enhances the decomposition of ethylene, CO_x selectivity, carbon balance and reduces the formation of unwanted by-products such as N₂O.

The effect of the presence of humidity in a gas stream on the removal of VOCs has to be considered for more realistic environmental and industrial applications. The presence of humidity in flue gasses can have both positive and negative effect on the decomposition of VOC and the product selectivity. The presence of humidity can modify the surface state of the packing material and quench the electrons which affects the discharge characteristics. The presence of water can greatly influence the chemical reactions by quenching electrons and other excited reactive species and by producing OH radicals.

Ogata et al. [46] reported that the presence of water (5%) reduces the decomposition efficiency of benzene, toluene and xylene in a BaTiO₃ packed bed DBD reactor. Urashima et al. [92] showed that the removal efficiency of C₂F₆ is reduced in the presence of humidity (relative humidity = 70%) due to the extra electron energy loss for the dissociation of water molecules. In [47,108], it is reported that the presence of humidity changes the surface states of BaTiO₃ in a PBDBD reactor, resulting in a reduced benzene removal efficiency. Wu et al. [68] reported that the presence of humidity (4.43 vol %) reduces the toluene removal efficiency due to quenching of high energy electrons by water and reducing the formation of active oxygen.

Zhu et al. [48] reported that the presence of humidity reduces the benzene removal efficiency due to the competitive adsorption of water on the surface of TiO₂. Wu et al. [68] reported that the presence of humidity reduces the toluene decomposition efficiency due to competitive adsorption of water on active sites of the catalyst. On the other hand, Zhao et al. [109] reported that the presence of humidity has no significant effect on the removal of formaldehyde using Ag/Cu-Hz as packing material due to the selective adsorption. Thus, the humidity tolerance of the PBDBD reactor depends on the ability of packing to selectively adsorb the pollutant.

The presence of humidity suppresses the formation of toxic by-products such as CO and NO_x and enhances CO₂ selectivity. For the reactor packed with BaTiO₃, the deactivation of lattice oxygen species in BaTiO₃ by H₂O reduces CO [46] and NO_x formation [108].

The lifetime of the packing material is very important for the commercialization of the PBDBD reactors for the abatement of VOC. The micro-pores of the porous material can get clogged by the accumulation of solid deposits resulting in a decrease in the decomposition efficiency of VOCs. In [107], it is reported that the accumulation of solid deposit on the surface of porous packing material (α-Al₂O₃) blocks the pores leading to the deactivation of the packing material. The activity of the porous material can be regenerated by an oxygen plasma treatment of the packing material [107]. On the other hand, the non-porous packing material does not show any time dependent deterioration in its performance [107]. In [67], it has been reported that the presence of TiO₂ enhances the benzene oxidation by decomposing ozone to form active oxygen. However, a poor carbon balance ($CB(\%) = \frac{[CO_x]}{6[C_6H_6]_{conv}} \times 100\%$) is obtained due to deposition of intermediates on the surface of TiO₂.

3.5. By-Product Formation

The production of toxic by-products during the abatement of VOC using NTP technology is one of the major concern for the commercialization of the discussed plasma technology for air purification. The most common by-products produced by an NTP reactor during the abatement of VOC in air are ozone, NO_x , aerosols and other VOCs. It has been widely reported in literature that the presence of the packing material reduces the formation of toxic by-products such as ozone and NO_x either by decomposition or by adsorption of the by-product and enhances CO_2 selectivity by complete oxidation of organic compounds.

The fact that the production of ozone is reduced in the presence of a packing material is mainly due to the decomposition of ozone on the surface of the packing material to form active oxygen species. The activity of active oxygen is higher than ozone and this results in an enhanced VOC removal efficiency. Chae et al. [45] mentioned that the production of ozone in a PBDBD reactor is 60% lower than in an unpacked reactor. Zheng et al. [88] reported that the formation of ozone is highly reduced in the DBD with a packing material when compared to an empty reactor. In [110], ozone formation is suppressed by the presence of $\text{TiO}_2/\text{Al}_2\text{O}_3/\text{Ni}$ foam when compared to unpacked reactor. Whereas Zhu et al. [48] showed that the presence of TiO_2 coated RR increases the ozone concentration enhancing benzene removal efficiency.

The CO_2 selectivity during the abatement of VOCs is enhanced by the complete oxidation of the organic compounds to form CO_2 and H_2O . The formation of CO_2 is enhanced by the presence of a porous packing material due to the adsorption of VOC in the pores which increases the VOC retention time in the discharge region resulting in deep oxidation of VOC. Ogata et al. [44,111] reported that the decomposition of benzene and CO_2 selectivity are enhanced in an $\text{Al}_2\text{O}_3/\text{BaTiO}_3$ packed reactor. Enhancement of CO_2 selectivity has also been reported for reactors packed with photocatalysts such as TiO_2/RR [48,53] and $\text{TiO}_2/\text{glass beads}$ [100]. Kim et al. [47] reported that a BaTiO_3 packed bed reactor inhibits the formation of aerosol by enhancing the oxidation of benzene to CO and CO_2 .

Ogata et al. [44] found that the presence of porous Al_2O_3 in $\text{Al}_2\text{O}_3/\text{BaTiO}_3$ in a hybrid PBDBD reactor suppresses the formation of N_2O . Zheng et al. [88] reported that the formation of NO_2 is highly reduced to 0.5 ppm in the DBD reactor packed with $\gamma\text{-Al}_2\text{O}_3$ when compared to an empty reactor. This is due to the adsorption of NO_2 on the surface of the packing material and only 0.5 ppm of NO_2 was produced.

The formation of yellow, brownish yellow or brownish solid deposit occurs on the wall of the DBD reactor which leads to a poor carbon balance during the abatement of VOC. The presence of packing material suppresses the formation of solid deposits by complete oxidation of the organic by-products. In [57], Gandhi et al. reported the formation of unwanted by-products such as acetylene and acetaldehyde from the decomposition of butane disappeared in the presence of glass wool loaded with TiO_2 or GO as packing material. In [112], Trinh et al. reported that the presence of MnO_2 coated monolith packing material inhibits the formation of polymer like deposit in the process of acetone abatement.

On the other hand, even in the presence of packing material, the formation of polymeric solid deposit is observed on the wall of the reactor and the surface of the packing material. During the decomposition of methane in the absence of O_2 , brown yellowish deposit was found in the inner electrode [113]. Decomposition of xylene in N_2 , BaTiO_3 packed bed reactor results in poor carbon balance due to the formation of a carbon deposit, polymer, decomposed fragment, cluster, or particulate [46]. During the process of decomposition of benzene in the absence of O_2 , carbonaceous deposit was found on the surface of the catalyst [114,115]. Thus, it is evident that N_2 plays an important role in the polymerization process and this problem can be rectified by using sufficient amount of O_2 in the feed gas [57].

4. Catalyst Loading on Packing Materials

Catalysts in single stage reactors are in direct contact with plasma. The plasma assisted reactions on the surface of the catalyst play an important role in addition to the gas phase reaction in VOC removal [75]. The pathway of destruction of one of the model VOC (i.e., Toluene) in FeO_x/SBA-15 packed bed DBD reactor is shown in Figure 7. As shown in the mechanism pathway, the destruction of toluene takes place: (i) in gas phase (by direct collision of toluene and other intermediate by-products with electron and other reactive species such as O•, OH•, N₂•, NO•, N₂O•) and (ii) on the surface of the catalyst (by the reaction between adsorbed toluene and other intermediate by-products with active species such as O• and OH•) [116]. The combined effect of the excellent toluene absorption capability of SBA-15 and O₂ absorption capacity of Fe²⁺ greatly increased the toluene removal efficiency, CO_x selectivity and remarkably reduced the formation organic byproducts. Thus, the key points for screening the catalyst for the abatement of VOCs are removal efficiency and carbon balance. In literature, it is shown that CO₂ selectivity is independent of SIE whereas the removal efficiency increases with increase in SIE. The initial decomposition of VOC is determined by the SIE applied, whereas the catalyst is crucial in the decomposition of the intermediates formed during the decomposition of VOC resulting in a better carbon balance. Thus, the catalyst loading on the packing materials improves the VOC removal efficiency [73], suppresses the formation of unwanted by-products like CO, NO_x [73], ozone [117] by deep oxidation of the intermediate by-products. The most commonly used catalyst in the PBDBD reactors for the abatement of VOCs are metal oxides such as CuO_x [18,68,73,117,118], MnO_x [67,68,73,81,105,117,119–121], CeO_x [18,68,74,105,117,122], CoO_x [117], NiO_x [68,117], FeO_x [116] and noble metal coated or impregnated porous or metal oxide catalysts.

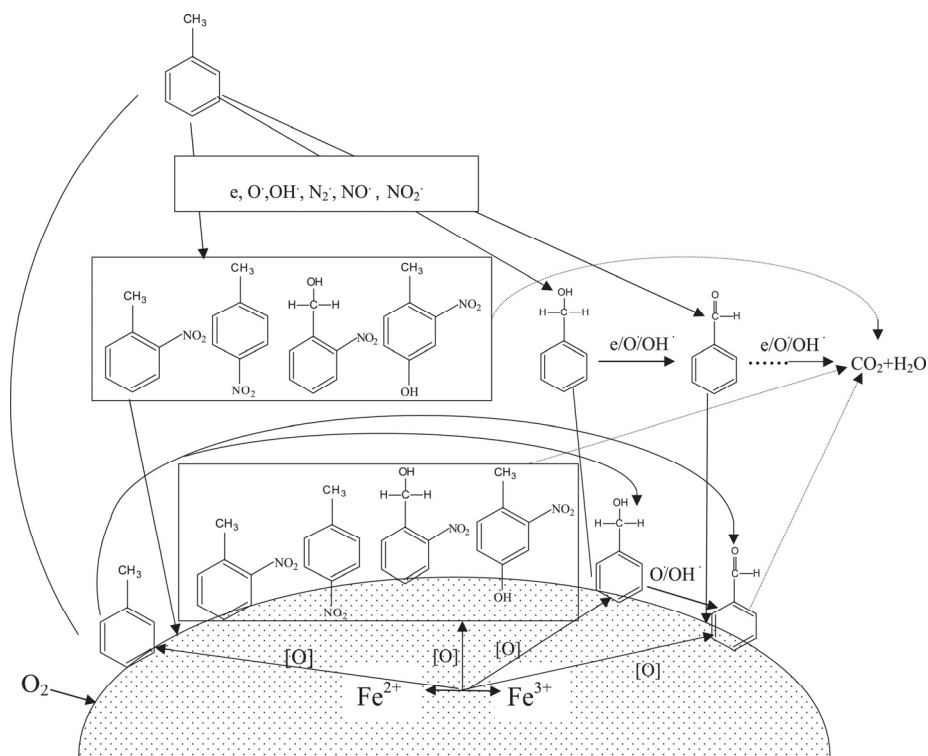


Figure 7. Pathways of toluene degradation in the gas phase and on the FeO_x/SBA-15 surface. Reprinted from [116]. Copyright (2017), with permission from Elsevier.

4.1. Removal Efficiency

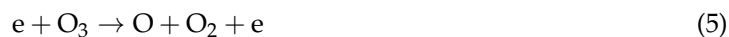
The transition metal oxides have lattice oxygen, surface oxygen and adsorbed oxygen [123,124] which play an important role in VOC oxidation in addition to the gas phase oxygen present in the flue gas [125,126]. Zhu et al. [118] reported that a better acetone removal efficiency was obtained for 5 wt % CuO/ γ -Al₂O₃ due to its higher reducibility and abundance of highly mobile oxygen species on the surface of the catalyst. In [18], it has been reported that the combination of plasma and Cu–Ce binary metal catalyst enhanced the removal efficiency of formaldehyde. This is mainly attributed to the enhanced oxygen vacancy and adsorbed oxygen on the pores of the surface of the catalyst which facilitate the redox reaction between Ce and Cu species in the catalyst. Zhu et al. [53] reported that the decomposition efficiency of benzene is improved by the presence of TiO₂ catalyst in a RR packed bed DBD reactor. In [121], it has been reported that WO₃ coated on TiO₂ has better removal efficiency of TCE when compared to V₂O₅ coated TiO₂; however the reason for this behavior is not explained in the article. In [96], it has been reported that the removal efficiency of TCE is enhanced by coating TiO₂ with V₂O₅.

Uniform dispersion of a metal catalyst on the packing material is very important for enhanced VOC removal efficiency due to the increase in the active metal surface [49]. Lu et al. [116] reported that loading SBA-15 with FeO_x enhances the toluene removal efficiency and CO₂ selectivity by reducing the unwanted by-products like benzaldehyde, benzyl alcohol, formic acid, acetic acid, benzenemethanol, tetradecane, hexadecane and heptadecane. The excellent toluene absorbing property of SBA-15 and oxygen absorbing property of Fe²⁺ ion generated by FeO_x are decisive in the abatement of toluene. 3% Fe loading is found to be optimal due to its high dispersion nature on the support material. In [68], it is shown that NiO loaded γ -Al₂O₃ enhanced the removal of toluene as NiO decomposes ozone to atomic oxygen much more efficiently when compared to other catalysts. The metal loading up to 5 wt % increases the removal efficiency whereas further increase in Ni loading decreases the decomposition efficiency. This is probably due to the formation of bulk NiO which starts screening the active sites as 5 wt % of Ni loading is closer to the threshold of monolayer dispersion of NiO on Al₂O₃. Kang et al. [127] reported that TiO₂ supported by Al₂O₃ shows better decomposition efficiency of toluene when compared to glass beads. This is because more TiO₂ is attached to Al₂O₃ than to glass beads and Al₂O₃ acts as an electron acceptor.

On the other hand, loading the porous support material with catalyst can affect the surface properties of the packing material by reducing the overall pore volume and surface area. Zhu et al. [117] reported that the removal efficiency of acetone is enhanced with MO_x/ γ -Al₂O₃ when compared to pure γ -Al₂O₃ even though the metal oxide supported alumina has smaller surface area ($S_{\text{BET}} = 148 \pm 2 \text{ m}^2/\text{g}$) when compared to pure alumina ($S_{\text{BET}} = 187 \text{ m}^2/\text{g}$). This emphasizes the role of catalytic activity of the metal oxides in the decomposition of VOCs. The catalytic activity of metal oxides is determined by their reducibility and the presence of oxygen on the surface of the catalyst. The acetone removal efficiency of CuO_x/ γ -Al₂O₃ is higher when compared to other metal oxides due to its higher reducibility and a carbon balance $\left(CB(\%) = \frac{3[\text{C}_3\text{H}_6\text{O}]_{\text{out}} + [\text{CO}] + [\text{HCOOH}] + [\text{CO}]_2 + [\text{HCHO}]}{3[\text{C}_3\text{H}_6\text{O}]_{\text{in}}} \times 100\% \right)$ higher than 95% is obtained due to the presence of surface oxygen species.

The presence of an oxidation catalyst as packing material plays an important role in the formation of active oxygen on the surface of the catalyst which enhances VOC removal efficiency. The active oxygen is formed from ozone by two different pathways as follows: (i) direct collision between active species and air molecules (Equations (4) and (5)) [105] and (ii) decomposition of ozone on the catalyst surface (Equation (6)). The amount of active atomic oxygen produced by the second pathway is dependent on the nature of the catalyst. In [119], it has been reported that the presence of MnO₂ enhances the decomposition of TCE and reduced the formation of by-products such as dichloro-acetylchloride (DCAC), phosgene and trichloro-acetaldehyde (TCAA). In [67], it has been reported that the presence of MnO₂ packing material enhances the decomposition of benzene. In [128], it is shown that the MnO₂ loaded γ -Al₂O₃ enhances the removal of toluene due to an enhancement of the redox reaction by MnO₂. In [105], it has been shown that CuO supported on MnO₂ enhances

the removal efficiency of chlorobenzene. Thus, MnO_2 accelerates the decomposition of ozone to form active O species resulting in an enhanced and complete oxidation of VOCs.



The removal efficiency of chlorobenzene and CO_2 selectivity are enhanced by a $\text{CeO}_2/\text{HZSM-5}$ packed reactor when compared with an unpacked reactor due to the good catalytic activity, the presence of oxygen vacancy and the oxygen activity of CeO_2 [105] and due to the high surface area and Brønsted acid sites of HZSM-5 [122]. The level of ozone in the exhaust is also reduced, probably due to the decomposition of ozone on the surface of the catalyst [129] and utilized for chlorobenzene conversion. In [65], it has been reported that the presence of $\text{V}_2\text{O}_5/\text{TiO}_2$ or Cu-ZSM-5 enhances the decomposition of TCE partly due to the adsorption of TCE on the packing material.

Kim et al. [41] studied the effect of Ag loading on TiO_2 on the decomposition efficiency of benzene and the carbon balance. The results showed that higher the silver content the better the carbon balance ($CB(\%) = \frac{[\text{CO}] + [\text{CO}]_2 + [\text{HCOOH}]}{n[\text{VOC}]_{\text{conv}}} \times 100\%$) is as silver aids the decomposition of intermediates formed on the surface of TiO_2 . However the decomposition efficiency starts to decline when the Ag loading is more than 4 wt %, as the loaded silver decreases the surface area of TiO_2 which is responsible for the initial decomposition of benzene. Whereas in [120], it is mentioned that the TiO_2 is more effective in benzene decomposition when compared to 0.5 wt % Ag impregnated TiO_2 . In the above mentioned works, although the Ag loading on TiO_2 is done by the impregnation method, the difference in the results can be explained by the difference in calcination (thermal treatment of catalyst in oxidation environment) temperature and calcination time of the catalyst. Kim et al. [41] studied the loading of different metals such as Ag and Ni on the TiO_2 packing material for the removal efficiency of benzene and carbon balance. Although Ni loaded TiO_2 showed higher removal efficiencies when compared to Ag, there was a problem of a poor carbon balance. This shows that Ni has lower catalytic reactivity towards the intermediates produced during the process and these intermediates are deposited on the surface of Ni/ TiO_2 .

Li et al. [50] studied the effect of Pt loading on $\gamma\text{-Al}_2\text{O}_3$ on the decomposition efficiency of benzene, CO_2 selectivity and formation of by-products. Pt/ $\gamma\text{-Al}_2\text{O}_3$ showed higher decomposition efficiency when compared to unloaded $\gamma\text{-Al}_2\text{O}_3$. This is because the presence of Pt increases the number of active sites and reduces the activation energy of the decomposition reaction. Pt/ $\gamma\text{-Al}_2\text{O}_3$ also suppresses harmful NO_x formation by (i) reducing the energy of electrons; thus reducing the number of excited N_2 , (ii) accelerate oxygen decomposition and oxidation. Also, the formation of CO is reduced in the presence of Pt/ $\gamma\text{-Al}_2\text{O}_3$ as Pt can promote O_3 decomposition resulting in enhanced CO oxidation. An et al. [62] studied the effect of metal (Cu) loading on molecular sieve and Cu, Co, Ag or Au loading on Al_2O_3 on the removal efficiency of toluene and formation of by-products and the results show that the metal loading enhances the removal efficiency by decomposition of ozone on the catalyst surface.

4.2. By-Product Formation

The formation of unwanted by-products such as CO, ozone, NO_x and other organic intermediates is one of the main disadvantages of NTP application for the abatement of VOCs. In the literature, it has been widely discussed that the metal catalysts loaded packing material plays an important role in the deep oxidation of VOCs resulting in increased CO_2 selectivity due to deep oxidation of the intermediate organic by-products.

The formation of CO is reduced by using Ni loaded BaTiO_3 as packing material when compared to a BaTiO_3 pellet packed bed reactor [71]. Apart from the enhanced removal efficiency, Pt-Pd loaded Al_2O_3 drive the oxidation of styrene towards CO_2 rather than the formation of CO [75]. In [51], it is

shown that loading HZSM-5 with Ag results in complete oxidation of benzene to CO₂ and only a very negligible amount of CO is produced. This is due to strong π -complexation of Ag with benzene [101]. Kim et al. [55] reported that the catalyst loading (Ag/Pt) on TiO₂ enhances CO₂ selectivity during benzene decomposition. However Pt loaded TiO₂ has a negative effect on the decomposition efficiency when compared to TiO₂. In [57], it is reported that glass wool loaded with TiO₂ or graphene oxide produced less CO and other organic by-products when compared to glass wool loaded with ZrO₂ or alumina. This is probably due to the photocatalytic properties of graphene oxide and TiO₂ which enhanced the formation of CO₂.

The amount of catalyst loading on the packing material plays an important role in CO₂ selectivity. Kim et al. [52] reported that CO₂ selectivity is independent of SIE when Ag loading is more than 0.5 wt %; whereas for Ag loading less than 0.3 wt %, CO₂ selectivity decreases with increase in SIE due to the deposit of intermediates on the packing material.

Ogata et al. [95] mentioned that the formation of N₂O during decomposition of benzene is greatly reduced by packing the DBD reactor with metal loaded porous Al₂O₃/BaTiO₃. Kim et al. [55] reported that the catalyst (Ag/Pt) loaded TiO₂ suppresses the formation of undesired by-product such as NO_x. An et al. [62] reported that NO_x produced by the plasma discharge during toluene decomposition is reduced by the presence of 1 wt % Au/Al₂O₃ as packing material. Pangilinan et al. [49] reported that the formation of ozone is reduced with Ag/TiO₂ and decreases with the increase in metal loading on the catalyst.

4.3. Catalyst Poisoning

The activity of the catalyst used as packing material in PBDBD reactor shows time dependent deterioration due to the accumulation of organic intermediates on the surface of the catalyst or absorption of certain organic compounds.

During the process of decomposition of benzene, toluene and xylene, the activity of MnO_x/Al₂O₃ shows a decreased conversion efficiency after 150 h of usage [130]. This is probably due to the formation of the organic intermediates which is mainly composed of saturated aldehydes and/or ketones, carboxylic acids, phenols, primary alcohols, acid amides and nitro-aromatic compounds on the surface of the catalysts [130]. In [122], Jiang et al. reported the deactivation of catalyst in CeO₂/HZSM-5 packing material which is used for decomposition of chlorobenzene after 75 h of usage. The deactivation is mainly due to the absorption and deposition of methyl and organic halide on the surface of the catalyst which covers the active sites of the catalyst. In [131], Ran et al. studied the catalytic activity of Ru/Al₂O₃ packing material used for the abatement of dichloromethane in PBDBD reactor and observed the deactivation of catalysts which is mainly due to the chlorine deposition. Zhu et al. reported slight deactivation of Cu1Ce1 catalyst after 5 h of usage for the abatement of formaldehyde [18]. This is due to the formation of coke on the surface of the catalyst which blocks the micropores [18].

As prolonging the service life of the catalyst is very important for practical application, a suitable method for the regeneration of deactivated catalyst is very important. In most of the cases, the activity of the catalyst is gained by calcination of the catalyst in the presence of O₂ or air flow. In [130], Fan et al. gained the activity of MnO_x/Al₂O₃ by calcination of catalyst in air stream at 773 K for 4 h and decomposition efficiency obtained by using the calcined catalyst showed that the catalyst was fully regenerated.

Table 1. Source of different VOCs and their effect on human and environment.

Compound	Sources	Health Disorder	Environmental Issues	Ref.
Methane	Unburned natural gas	Breathing problem	Greenhouse gas	[132,133]
Butane	Fuel, fuel additive, aerosol propellant, refrigerant, chemical feedstock	Drowsiness, euphoria, fluctuation in blood pressure, memory loss, irregular heartbeat	Affects aquatic ecosystem	[57]
Ethylene (Ethene)	Engine exhaust, petrochemical derivative, thermal power plant, food industry, production facility of polymers and other chemicals	Anesthetic illness	Photochemical smog, ground level ozone	[102,134–137]
Hexane	Solvent in industry, gasoline vehicles	Nausea, vertigo, bronchial and intestinal infection, affects central nervous system and can be fatal	Haze	[91]
Benzene	Petrochemical waste gas, unleaded gasoline, production of ethylbenzene and styrene	Drowsiness, dizziness, unconsciousness, anemia, leukemia, blood diseases, Carcinogen, affects central nervous system and cause respiratory disorder	Smog, affects aquatic ecosystem, contaminates water and soil	[48,49,69,73,138–141]
Toluene (Methyl benzene)	As a solvent for production of paints, paint thinners, nailpolish, medicines, dyes, explosives, detergents, spot removers, lacquers, adhesives, rubber, antifreeze, printing, leather tanning, pharmaceutical industry, feedstock in chemical processes	Tiredness, confusion, weakness, memory loss, nausea, loss of appetite, hearing loss, loss of color vision, sleepiness, unconsciousness and death	Stratospheric ozone depletion, climatic changes, affects the potable and agricultural water	[38,127,128,142–144]
Styrene (Vinyl benzene)	Petrification material for resin, plastic and medicine	Memory loss, difficulties in concentration and learning, brain and liver damage, mutagen and potential carcinogen	Affects aquatic organisms and ground water, forms ground level ozone	[75,145]
Xylene (dimethyl benzene)	Solvent and fixative in pathology laboratories	Eye, nose and throat irritation, difficulty in breathing, impaired lung function, central nervous system impairment and adversely affects the nervous system	Pollutes the ground water	[146–149]
Formaldehyde	Production facilities of urea-formaldehyde, phenol-formaldehyde resins and some building materials such as plywood, chip board and paneling, adhesives, resins, preservatives, cosmetics, incomplete combustion in power plants and automobiles, incinerators	Irritation of eyes and respiratory tracts, nausea, headache, fatigue, dullness, thirst and suspected carcinogen	Detrimental to vegetation	[42,72,74,150–153]
Acetaldehyde	Tobacco smoke, production facilities of acetic acid, pyridine and pyridine base, peracetic acid, pentaerythritol, butylene glycol and chloral	Irritation of eye, nose and throat, causes conjunctivitis, coughing, central nervous system depression, eye and skin burns, dermatitis and delayed pulmonary edema	Photochemical smog	[60,78]
Acetone (2-propanone)	Chemical production processes, vehicle emission, tobacco smoke, incineration of waste materials and as a solvent in cleaning and painting	Dizziness, unconsciousness, nausea	Oxygen depletion in aquatic system	[88,117,118,154]

Table 1. Cont.

Compound	Sources	Health Disorder	Environmental Issues	Ref.
Perfluoroethane	Etching process and cleaning of process chambers in semiconductor industry	Affects respiratory system	Affects vegetation growth and fresh water lakes, greenhouse effect	[90,92,98,155]
Bromomethane (Methyl bromide)	Fumigant on agricultural fields and quarantine facilities	Headache, nausea, vomiting, dizziness, blurred vision, impairment of coordination, twitching, permanent debilitation or death, carcinogen (excessive exposure)	Depletes stratospheric ozone layer	[156–159]
Carbon tetrachloride	Solvent in industrial chemicals	Hepatic injury	Depletes stratospheric ozone layer	[71,160,161]
Dichloromethane	Solvent in various industrial applications	Headache, nausea, dullness, dizziness, pulmonary irritation, affects the central nervous system; abortion, affect the birth weight, carcinogen (excessive exposure)	Stratospheric ozone depletion, climatic changes	[38,162–164]
Chlorobenzene	Production of phenol and dichloro-diphenyl-trichloroethane (DDT), high boiling solvents, precursor for 2-nitrophenol synthesis, solvent in pharmaceutical and dye industries	Nervous and kidney damage, dizziness, neurasthenia, increase the risk of cancer	Precursor of secondary aerosols, photochemical smog	[19,81,105,122,165–167]
Trichloroethylene	Washing agent to remove oil and hydrophobic contaminants	Carcinogenic, nerve paralyzing, sick house syndrome	Depletion of ozone	[37,65,121]

Table 2. Overview of published papers on abatement of VOCs using packed bed non-thermal plasma reactors.

Compound	Packing Material	Size/Shape	Dielectric Constant	Carrier Gas	Flow Rate ¹ (L/min)	Initial Conc. ² (ppm)	Removal Efficiency (%)	Energy Density/Frequency	By-Products	Ref.
Methane (CH ₄)	BaTiO ₃	φ1 mm/sphere	5000	N ₂	1	1000	66	10 kJ/L (50 Hz)	–	[156]
	BaTiO ₃	φ1 mm/sphere	15,000	Air N ₂	0.2	1000	17 34	11 W 11 W (50 Hz)	NO _x , N ₂ O, NH ₃ , HCN, C ₂ H ₂	[168]
	No packing	–	–	2.5% + O ₂ + He	200 cm ³ /min	2500	32	165 J/L	–	[132]
	2 wt % Pd/SiO ₂	φ0.45–0.6 mm/sphere	3.9				35	169 J/L		
2 wt % Pd/TiO ₂	“ ³ ”	80	30				172 J/L			
2 wt % Pd/Al ₂ O ₃	“	9	54				163 J/L (4 kHz)			
Butane (CH ₃ CH ₂ CH ₂ CH ₃)	No packing	–	–	N ₂ + O ₂ (5%)	1	2000	65.56	100 W (400 Hz)	N ₂ O, CH ₃ CHO	[57]
	GW	–	–				90.37			
	TiO ₂ /GW	φ3 mm/sphere	–				90.31			
	α-Al ₂ O ₃	φ3 mm/sphere	–				83.97			
	ZrO ₂	φ3 mm/sphere	–				84.83			
GO/GW ⁴	–	–	85.60							
	BaTiO ₃	φ1 mm/sphere	–	Dry N ₂ Humid N ₂ (2%) Dry air Humid air (2%)	0.5	1000	89 90 88	8 kV (50 Hz)	CH ₄ , C ₂ H ₆ , CH ₂ =CH ₂ , CH ₃ CHOC ₃ H ₈ , CH ₂ =CHCH ₃ , Butenes, CH ₃ (CH ₂) ₂ CHO, CH ₃ CCH ₂ CH ₃ , Ethyloxirane, 2,3-dimethyloxirane, CH ₃ COCH ₃ , CH ₃ CHO, Methyl ether, Butanols, CH ₃ CN, CH ₃ NO ₂ , NO, N ₂ O, NO ₂	[169]

Table 2. Cont.

Compound	Packing Material	Size/Shape	Dielectric Constant	Carrier Gas	Flow Rate ¹ (L/min)	Initial Conc. ² (ppm)	Removal Efficiency (%)	Energy Density/Frequency	By-Products	Ref.						
Ethylene (CH ₂ =CH ₂)	No packing	–	–	Air	1	1898	78	1819 J/L	–	[107]						
	α -Al ₂ O ₃	–	9				100	1013 J/L	N ₂ O							
	SiO ₂	–	3.9				100	1054 J/L	N ₂ O							
	ZrO ₂	–	25				99	1932 J/L	CH ₄ , C ₂ H ₂ , HCHO, N ₂ O							
	GW	–	3.4				100	1900 J/L (400 Hz)	CH ₄ , C ₂ H ₂ , HCHO, N ₂ O							
	Non-porous α -Al ₂ O ₃	–	9.4				99	80 W	N ₂ O, HCHO, CH ₃ CHO							
Propylene	Porous α -Al ₂ O ₃	–	9.4	5% O ₂ + N ₂	1	1898	100	45 W	–	[102]						
	Porous zeolite	–	–				100	45 W (400 Hz)	N ₂ O, polymer like deposit							
	Glass beads	ϕ 5 mm/sphere	–				Dry air	10 20	150		79 60	5.5 W (60 Hz)	–	[59]		
Hexane	No packing	–	–	N ₂ + 15% O ₂	0.5	293–367	64	399 J/L	2-hexanone, 3-hexanone	[91]						
	Quartz	ϕ 1.79–2.29 mm/sphere	3.9				59	415 J/L								
	Al ₂ O ₃	“	–				67	422 J/L								
	Porous Al ₂ O ₃	“	9.9				70	389 J/L								
Benzene (C ₆ H ₆)	2 wt % Ni/TiO ₂	ϕ 1.8 mm/sphere	–	Air (100 °C)	4–10	200	93	210 J/L	NO ₂ , N ₂ O, Ozone	[41]						
	2 wt % Ag/TiO ₂	ϕ 1.8 mm/sphere	–				86	215 J/L								
	0.5 wt % Ag/ γ -Al ₂ O ₃	ϕ 2 mm/sphere	–				83	240 J/L								
	0.5 wt % Pt/ γ -Al ₂ O ₃	ϕ 3.2 × 3.6 mm/cylinder	–				95	210 J/L								
	0.5 wt % Pd/ γ -Al ₂ O ₃	ϕ 3.2 × 3.6 mm/cylinder	–				78	240 J/L								
	2 wt % Ag/H-Y	ϕ 1.5 × ~5 mm/cylinder	–				76	200 J/L								
	Ferrierite	ϕ 1.5 × ~5 mm/cylinder	–				79	200 J/L (500 Hz)								
	BaTiO ₃	ϕ 5 mm/sphere	–				–	1			500	>51	30 W	–	[45]	
	BaTiO ₃ pellets	–	–				4000	Dry air Humid air N ₂ Humid N ₂			0.2	200	60	2 W (50 Hz)	C ₂ H ₂	[46]
													42			
40																
BaTiO ₃	ϕ 2 mm/sphere	10,000	Dry air Humid air (4500 ppm)	0.2–3	200	52.9 37.1	386 J/L 384 J/L	HCOOH	[47]							
Ag/TiO ₂	ϕ 2 mm/sphere	–	Dry air Humid air (4500 ppm)			89.1 86	383 J/L 391 J/L									
No packing	–	–	–	–	–	–	54	12 kV/cm	–							
TiO ₂ /RR	ϕ 5 mm/sphere 10 mm (length) 1 mm wall Thickness	–	–	Dry air	1.6	1300 mg/m ³	80	13.6 kV/cm	Ozone	[48]						
3% Ag/TiO ₂	ϕ 1.4–1.7 mm/sphere	–	–	O ₂	0.55	200	100	10 J/L (50 Hz)	Ozone	[49]						
γ -Al ₂ O ₃	ϕ 2–3 mm/sphere	–	–	Air	3	320	80	800 J/L (8 kHz)	NO ₂ , NO	[50]						
Pt/ γ -Al ₂ O ₃	ϕ 2–3 mm/sphere	–	–				89									
1 wt % Ag/TiO ₂	ϕ 1.8 mm/sphere	–	100 °C	Dry air T = 100 °C	4	203–210	92.5	236 J/L	HCOOH, NO ₂ , N ₂ O	[52]						

Table 2. Cont.

Compound	Packing Material	Size/Shape	Dielectric Constant	Carrier Gas	Flow Rate ¹ (L/min)	Initial Conc. ² (ppm)	Removal Efficiency (%)	Energy Density/Frequency	By-Products	Ref.
	RR ⁵					600 mg/m ³	78	10 kV/cm		
	TiO ₂ /RR	φ5 × 10 mm/cylinder	–	Dry air	14 mm/s	1500 mg/m ³ 600 mg/m ³ 1500 mg/m ³	89 98 98	14 kV/cm 10 kV/cm 14 kV/cm (60 Hz)	Ozone, Aromatic polymers	[53]
	Glass	φ 2 mm/sphere	–	Dry air	0.5	400	49	10 W	–	[54]
	BaTiO ₃	φ2 mm/sphere	10,000				64	400 J/L		
	TiO ₂	φ1.8 mm/sphere	–	Dry air	2	203–210	81	390 J/L	–	
	1 wt % Ag/TiO ₂	φ1.8 mm/sphere	–				88	380 J/L		[55]
	1 wt % Pt/TiO ₂	φ1.8 mm/sphere	–				78	390 J/L (100 Hz–1.5 kHz)		
	Glass	φ3 mm/sphere	–	Dry air	–	240	34	25 kV	hydroquinone, heptanoic acid, 4-nitrocatechol, phenol, 4-phenoxy-phenol	[56]
	BaTiO ₃	φ2 mm/sphere	4000	Humid air (0.5%)	0.2	200	96.8	5.2 W (50 Hz)	C ₂ H ₂ , Ozone, N ₂ O, HNO ₃	[66]
	No packing	–	–		0.5		34	350 J/L		
	MnO ₂	φ1.18–1.7 mm/sphere	–	Air	“	100	41	360 J/L	–	[67]
	TiO ₂	φ1.7 mm/sphere	–		0.1		45	300 J/L (50 Hz)		
	1 wt % Ag/TiO ₂	φ1.8 mm/sphere	–	Dry air N ₂ Ar-O ₂	4	200	81.5 94.5 96	197 J/L 247 J/L 94 J/L	NO ₂ , N ₂ O, HCOOH	[69]
	CuO/AC ⁶	–	–				90.6			
	AC	–	–	Humid air (50%)	18,857 h ^{−1}	240	70.5	70 J/L	NO _x	[73]
	MnO/AC	–	–				>85			
	MnO ₂ /AC	–	–				>85			
	BaTiO ₃	φ2 mm/sphere	15,000				98.8	8 W		
	SrTiO ₃	φ2 mm/sphere	2600	Dry air	0.2	200	99.7	8 W	NO _x , N ₂ O, C ₂ H ₂ , Ozone	[86]
	CaTiO ₃	φ2 mm/sphere	200				65.3	6.7 W		
	Mg ₂ TiO ₄	φ2 mm/sphere	20				6	7.6 W (50 Hz)		
	Al ₂ O ₃ /BaTiO ₃	φ2 mm/φ1 mm/sphere	10/5000	Humid air (0.5%)	0.2	200	100	3 kJ/L	–	[95]
	BaTiO ₃	φ2 mm/sphere	5000				~100	2.6 kJ/L		
	CaTiO ₃	φ2 mm/sphere	200				70	2 kJ/L		
	No packing	–	–	Air	0.2	100	40	140 J/L (900 Hz)	C ₆ H ₅ OH	[100]
	TiO ₂ /Glass beads	φ5 mm/sphere	–				50			
	BaTiO ₃	φ2 mm/sphere		Humid air (0.5%)	0.2	200	74			
	BaTiO ₃ /Al ₂ O ₃	φ2 mm/φ1 mm/sphere	4000				87	6 W (50 Hz)	N ₂ O, NO _x , C ₂ H ₂	[44]
	BaTiO ₃	φ1 mm/sphere		Humid air (0.5%)	0.2	200	80			
	MS-3A/BaTiO ₃	φ2 mm/φ1 mm/sphere	4000				72	6 W (50 Hz)	N ₂ O	[104]
	MS-4A/BaTiO ₃	“					74			
	MS-5A/BaTiO ₃	“					85			
	MS-13X/BaTiO ₃	“					100			
	BaTiO ₃	φ2 mm/sphere	4000	Humid air (0.5%)	0.2	200	79	6 W (50 Hz)	N ₂ O, NO _x , C ₂ H ₂	[111]
	Al ₂ O ₃	φ1 mm/sphere	–				88.5			

Table 2. Cont.

Compound	Packing Material	Size/Shape	Dielectric Constant	Carrier Gas	Flow Rate ¹ (L/min)	Initial Conc. ² (ppm)	Removal Efficiency (%)	Energy Density/Frequency	By-Products	Ref.
Toluene (C ₆ H ₅ CH ₃)	BaTiO ₃	φ2 mm/sphere	4000	Dry air Humid air (1%) N ₂ Humid N ₂ (1%)	0.2	200	97 83 93 77	9 W 9 W 8 W 10 W (50 Hz)	N ₂ O, NO ₂ , C ₂ H ₂	[108]
	No packing BaTiO ₃	– φ5 × 5 mm/cylinder	– –	Air	0.5	400	52 73.5	340 J/L 498 J/L	–	[138]
	Glass	φ5 mm/sphere	–	–	–	–	70.8 67	468 J/L 400 J/L (50 Hz)	–	–
	No packing MnO ₂	– –	– –	Dry air	0.4	1000	39 58	42 kV (50 Hz)	–	[119]
	BaTiO ₃ pellet	φ1 mm/sphere	5000	Dry air	0.8 0.2	60 57	100 100	14 kV 8 kV (60 Hz)	Ozone	[38]
	0.5 wt % Pt/γ-Al ₂ O ₃ 2 wt % Ag/TiO ₂	– –	– –	Air	4–10	150	98 92	210 J/L (500 Hz)	–	[41]
	BaTiO ₃ beads	–	4000	Dry air Humid air N ₂ Humid N ₂	0.2	200	66 59 45 37	2 W (50 Hz)	CH ₄ , C ₆ H ₆ , C ₆ H ₅ CH ₃ , C ₂ H ₂	[46]
	Glass beads	–	–	Dry air	0.315	240	36	172 J/L (110 Hz)	C ₆ H ₅ COOH	[58]
	Glass beads	φ5 mm	–	Air	5 " 2 "	200	30 50 57.5 76	5.5 W 11 W 5.5 W 11 W (60 Hz)	–	[59]
	RR NaNO ₂ /RR BaTiO ₃ /RR	φ9.2 mm × 10.5 mm/cylinder " "	– – –	Humid air (30%)	8.5	–	93 95 98	687 J/L 786 J/L 818 J/L 25 kHz)	Ozone	[61]
	No packing OMS-2 10 wt % Cu/OMS-2 Al ₂ O ₃ 1 wt % Au/Al ₂ O ₃ Nb ₂ O ₅	– – – – – –	– – – – – –	Air	0.06	800	60 70 80 75 90 96	–	CH ₂ O ₂ , C ₂ H ₄ O ₂ , C ₆ H ₆ , C ₆ H ₅ CH ₂ OH, C ₆ H ₅ COOH, 5-methyl-2-nitrophenol (as deposit)	[62]
	No packing Glass Ceramic RR Al ₂ O ₃ BaTiO ₃ /Al ₂ O ₃ TiO ₂ /Al ₂ O ₃ BaTiO ₃ /TiO ₂ /Al ₂ O ₃	– – – – – – –	– – – – – – –	Air	10	700 mg/m ³	36 45 58 72 59 52 71	280 J/L 330 J/L 350 J/L 380 J/L 360 J/L 390 J/L 340 J/L (50–500 Hz)	–	[43]
	No packing Ceramic RR	– φ5 mm/cylinder	– –	Air	0.33	1200 mg/m ³	72 97	660 J/L 450 J/L (50 Hz)	Ozone	[63]
	No packing NiO/γ-Al ₂ O ₃ MnO ₂ /γ-Al ₂ O ₃ CeO ₂ /γ-Al ₂ O ₃ Fe ₂ O ₃ /γ-Al ₂ O ₃ CuO/γ-Al ₂ O ₃ γ-Al ₂ O ₃	– – – – – – –	– – – – – – –	Air	0.1	6	48 88.8 78.8 77.1 73.2 70.7 63.5	9 J/L 50 Hz)	C ₆ HCH ₂ OH, C ₆ H ₅ CHO, C ₆ H ₅ COOH	[68]

Table 2. Cont.

Compound	Packing Material	Size/Shape	Dielectric Constant	Carrier Gas	Flow Rate ¹ (L/min)	Initial Conc. ² (ppm)	Removal Efficiency (%)	Energy Density/Frequency	By-Products	Ref.
	No packing Glass pellets	– φ5 mm	– 5	Humid air (95%)	1	500	66 91	11.6 kV (60 Hz)	N ₂ O	[79]
	No packing Glass pellets TiO ₂ /glass pellets	– φ5 mm "	– – –	Air	0.6	1100	35 78 77	11 W 9 W 10 W (60 Hz)	–	[80]
	No packing TiO ₂ /Al ₂ O ₃ /Ni foam	– –	– –	Air	0.2	50	74 94	1527 J/L	Ozone	[110]
	Glass beads 3 wt % TiO ₂ /glass beads TiO ₂ /γ-Al ₂ O ₃	– – –	– – –	O ₂	4	1000	40 70 80	13 kV (60 MHz)	–	[127]
	γ-Al ₂ O ₃ TiO ₂ /γ-Al ₂ O ₃ 5 wt % MnO ₂ /γ-Al ₂ O ₃ 10 wt % MnO ₂ /γ-Al ₂ O ₃ 15 wt % MnO ₂ /γ-Al ₂ O ₃	– – 5–7 mm/sphere – –	– – – – –	Air	2	1000 mg/m ³	75 88 85 98 98	0.7 kJ/L (150 Hz)	Ozone	[128]
	No packing γ-Al ₂ O ₃	–	–	Air	0.1	200 215	50 53	4 W (12.5 kV)	–	[103]
	No packing	–	–	N ₂ N ₂ + 3% O ₂ Air			43 51 27			
	SBA-15	–	–	N ₂ N ₂ + 3% O ₂ Air N ₂ N ₂ + 3% O ₂	0.3	100	50 86 92 61 98	192 J/L (50 Hz)	–	[116]
	3% FeO _x /SBA-15 SiO ₂	– –	– –	Air N ₂ Air			97 50 45			
Styrene (C ₆ H ₅ CH=CH ₂)	No packing Glass Al ₂ O ₃ Pt-Pd/Al ₂ O ₃	– φ5 mm " "	– – – –	Dry air	0.6	408	9 50 70 96	14 kV (60 Hz)	C ₆ H ₆ , Toluene, Benzene acetaldehyde	[75]
	No packing γ-Al ₂ O ₃ P25/γ-Al ₂ O ₃ TiO ₂ /γ-Al ₂ O ₃	– – – –	– – – –	Dry air	0.5	1000 mg/m ³	54 70 89 97	12.5 kV (10 kHz)	NO, NO ₂	[170]
	BaTiO ₃	φ5 mm	–	–	1	490	95	28 W	–	[45]
Xylene (C ₆ H ₄ (CH ₃) ₂)	BaTiO ₃ pellets	–	4000	Dry air Humid air N ₂ Humid N ₂	0.2	200	76 71 49 49	2 W (50 Hz)	CH ₄ , C ₆ H ₆ , C ₆ H ₅ CH ₃ , C ₂ H ₂	[46]
Formaldehyde (HCHO)	No packing α-Al ₂ O ₃ γ-Al ₂ O ₃	– – –	– – –	Humid air (1%) T = 70 °C	0.605	140	77 84 95	108 J/L (50 Hz)	NO, NO ₂ , N ₂ O, HCOOH	[42]

Table 2. Cont.

Compound	Packing Material	Size/Shape	Dielectric Constant	Carrier Gas	Flow Rate ¹ (L/min)	Initial Conc. ² (ppm)	Removal Efficiency (%)	Energy Density/Frequency	By-Products	Ref.			
	No packing	–	–	Humid air (30%)	8.5	50 mg/m ³	70	670 J/L	Ozone	[72]			
	3000 ppm NaNO ₂ /RR	φ9.2 × 10.5 mm/cylinder	–				75	678 J/L					
	5000 ppm NaNO ₂ /RR	“	–				80	664 J/L					
	8000 ppm NaNO ₂ /RR	“	–				86	656 J/L (15 kHz)					
	Ag/CeO ₂ pellets	–	–	–	Humid air (1%)T = 70 °C	0.605	276	99	108 J/L (50 Hz)	NO, N ₂ O, NO ₂	[74]		
								99					
								78					
	Fused silica	–	–	–	–	–	–	57	–	–	–		
								72					
								66					
	No packing	–	–	–	Dry air	1	57.7	44	645 J/L	HCOOH	[18]		
								91	615 J/L				
94								575 J/L					
87								583 J/L					
94								485 J/L					
87								530 J/L (10 kHz)					
No packing	–	–	–	Dry air	0.2	102	93	40 W	–	[171]			
							99	42 W (9 kHz)					
Acetaldehyde (CH ₃ CHO)	γ-Al ₂ O ₃	φ5 mm	–	5% O ₂ , N ₂	1	1000	100	46 W (60 Hz)	N ₂ O, NO ₂ , CH ₃ NO ₂ , CH ₃ NO ₃ , HCN, CH ₃ OC ₂ O ₅ , CH ₃ COOH, CH ₃ OH	[60]			
	BaTiO ₃ pellets	φ1.7–2 mm	10,000	Humid air (4%)	–	100	92	16 kV	Ozone, NO (low), NO ₂ (low), N ₂ O (low)	[82]			
							96	18 kV					
	BaTiO ₃ pellets	φ1.7–2 mm	10,000	10,000	Humid air (2%)	–	100	97	14 kV	NO (low), NO ₂ (low), N ₂ O (low)	[78]		
								88	16 kV (60 Hz)				
	No pellet	–	–	–	Dry air	1	100	87	5.8 W	–	–		
92								2.4 W					
BaTiO ₃ pellets	φ1.7–2 mm	10,000	10,000	Humid air (2%)	–	100	79	2.4 W	–	–			
							79	2.4 W					
Acetone (CH ₃ COCH ₃)	No packing	–	–	Dry air	0.2	100	40.83	441 J/L	NO ₂ , N ₂ O, Ozone	[88]			
	Glass pellets	φ1 mm	3.9				54.01	534 J/L					
	α-Al ₂ O ₃	–	9.5				59	566 J/L					
	γ-Al ₂ O ₃	–	12.6				80	640 J/L (50 Hz)					
	γ-Al ₂ O ₃	–	–	–	Dry air	1	1184	64.1	1287 J/L	HCHO, HCOOH	[117]		
								10 wt % CuO _x /γ-Al ₂ O ₃	–			94.3	1012 J/L
								10 wt % CeO _x /γ-Al ₂ O ₃	–			76	1036 J/L
								10 wt % CoO _x /γ-Al ₂ O ₃	–			89	1047 J/L
								10 wt % MnO _x /γ-Al ₂ O ₃	–			89	1051 J/L
								10 wt % NiO _x /γ-Al ₂ O ₃	–			79	1051 J/L (10 kHz)
	γ-Al ₂ O ₃	–	–	12.6	Dry air	–	500 mg/m ³	58	25 W (10.2 kHz)	HCOOH, HCHO, NO ₂ , N ₂ O	[118]		
								2.5 wt % CuO/γ-Al ₂ O ₃				–	65
5 wt % CuO/γ-Al ₂ O ₃								–				68	
7.5 wt % CuO/γ-Al ₂ O ₃								–				64	
10 wt % CuO/γ-Al ₂ O ₃								–				58	
No packing	–	–	–	Dry air	0.6	1100	15	19 W	–	[80]			
							Glass	φ5 mm			45	16 W	
							TiO ₂ /glass	“			47	15 W (60 Hz)	

Table 2. Cont.

Compound	Packing Material	Size/Shape	Dielectric Constant	Carrier Gas	Flow Rate ¹ (L/min)	Initial Conc. ² (ppm)	Removal Efficiency (%)	Energy Density/Frequency	By-Products	Ref.
Perfluoroethane (CF ₃ -CF ₃)	BaTiO ₃	φ3.3 mm/sphere φ3.2 mm × 4 mm/cylinder	10,000	N ₂	0.03	3000	7 12	1 W (60 Hz)	-	[90]
	BaTiO ₃	φ3.2 mm × 4 mm/cylinder	10,000	N ₂	1	1500 3000	75 77	14 kV 15 kV (60 Hz)	CF ₄ , CHF ₃	[98]
	BaTiO ₃	φ3 mm/sphere	10,000	Dry N ₂ Humid N ₂ (70%)	0,025	3000	45 13	12 kV (60 Hz)	CF ₄ , NO ₂ , N ₂ O, SiF ₄	[92]
Bromomethane (CH ₃ Br)	BaTiO ₃	φ1 mm	5000	N ₂	1	1000	100	11 kJ/L	CH ₄ , CH ₂ Br ₂ , BrCN	[156]
				Humid N ₂ (2%)			88	14 kJ/L		
				Air			74	13 kJ/L		
				Humid air (2%)			70	14 kJ/L (50 Hz)		
Carbon tetrachloride (CCl ₄)	No pellet	-	-	Dry air	0.2	450-560	47.1	4.24 kV	-	[71]
	BaTiO ₃ pellets	φ1 mm	-				100	4.24 kV		
	Ni/BaTiO ₃	"	-				100	4.1 kV		
	SrTiO ₃ pellets	"	-				93-100	3.76 kV (18 kHz)		
Dichloromethane (CH ₂ Cl ₂)	BaTiO ₃	φ1.4-2.8 mm	-	N ₂	1	500	54	1000 J/L (100Hz)	HCN, HCl, CCl ₄ , N ₂ O, COCl ₂ , NOCl, COCl ₂ , HCN, HCl, CCl ₄ , COCl ₂ , HCl, COCl ₂	[163]
				Air			55			
				N ₂ + 3% O ₂			74			
				Ar			70			
				Ar + 21% O ₂			90			
BaTiO ₃	φ5 mm	-	-	1	460	89	28 W	-	[45]	
BaTiO ₃	-	2000-10,000	-	N ₂ + 3% O ₂	1	500	75	900 J/L (=15 W) (20 kHz)	N ₂ O, NO ₂ , NO, ClNO	[76]
BaTiO ₃	φ3.5 mm	-	-	N ₂ Air	1	500	18 12	66 J/L (= 1.1 W) (10 kHz)	HCN, Cl ₂ , HCl, COCl ₂ , N ₂ O, NO ₂ , HCl, Cl ₂	[77]
BaTiO ₃	φ3.5 mm	-	-	Air	1	500	27	1.1 W	HOCl, NO, NO ₂ , N ₂ O	[172]
γ-Al ₂ O ₃ /BaTiO ₃	φ3.5 mm	-	-	-	-	36	0.9 W (10.25-13.25 kHz)			
Chlorobenzene (C ₆ H ₅ Cl)	No packing	-	-	Dry air	0.36	1250 mg/m ³	84	7 kJ/L (10 kHz)	-	[122]
	CeO ₂ /HZSM-5	φ0.3-0.5 mm	-				96			
	No packing	-	-				32			
	CuO/MnO ₂	φ0.3-0.5 mm	-				70			
	CeO ₂ /HZSM-5	-	-				72			
Ag/TiO ₂	-	-	53							
No packing	-	-	-	Dry air	0.7	425	33	1280 J/L	-	[81]
MS-4A	φ2 mm	-	29				960 J/L			
6 wt % MnO ₂ /ALP	-	-	415				960 J/L (50 Hz)			

Table 2. Cont.

Compound	Packing Material	Size/Shape	Dielectric Constant	Carrier Gas	Flow Rate ¹ (L/min)	Initial Conc. ² (ppm)	Removal Efficiency (%)	Energy Density/Frequency	By-Products	Ref.
Trichloroethylene (Cl ₂ C=CHCl)	No packing	–	–	Dry air	0.4	1000	93	0.9 W	–	[65]
	V ₂ O ₅ /TiO ₂	φ5 mm/sphere	–				98	0.3 W		
	Cu-ZSM-5	φ3–6 mm × 1 mm thick/disc	–				96	0.1 W (50 Hz)		
	No packing	–	–	Dry air	0.4	1000	83	0.4 W	Ozone	[121]
	TiO ₂	φ2–3 mm/sphere	–				91	0.6 W		
	V ₂ O ₅ /TiO ₂	“	–				94	0.6 W		
	WO ₃ /TiO ₂	“	–	95	0.5 W (50 Hz)					
	No packing	–	–	Dry air	0.4	100	97	1.4 W	CH ₃ COOH, C ₂ H ₂ Cl ₃ NO	[96]
	TiO ₂	φ0.5–1 mm	–				98	1 W		
	TiO ₂	φ2–3 mm	–				96	0.6 W		
	TiO ₂	φ4–5 mm × 1 mm (disk)	–	98	0.4 W (50 Hz)					
	No packing	–	–	Dry air	0.4	1000	90	0.5 W	Cl ₂ HC-COCl	[119]
MnO ₂	–	–	95				0.6 W (50 Hz)			
BaTiO ₃	φ1 mm/sphere	–	–	Humid air (2%) N ₂	1	1000	86	5.1 kV/cm	Ozone, NO, NO ₂	[70]
							70	5.2 kV/cm		
							94	3.9 kV/cm		

¹ The unit of flow rate is L/min (unless and otherwise specified); ² the unit of initial conc. is ppm (unless and otherwise specified); ³ “ = same as previous line; ⁴ GO, graphene oxide, GW, glass wool; ⁵ RR, Raschig rings; ⁶ AC, activated carbon.

5. Conclusions

In this paper, an overview of the literature on packed bed dielectric barrier discharge (PBDBD) reactors for the abatement of volatile organic compounds is presented. The configuration of the packed bed DBD reactors such as the powered electrode, ground electrode and the power supply play an important role in determining the energy efficiency of the reactor. Using bolt as high voltage electrode enhances the electric field due to the presence of sharp edges and increases the number of microdischarges. Silver paint as ground electrode is advantageous as it avoids the formation of corona discharge in the voids outside the reactor. Thus, bolt as high voltage electrode and silver paint as ground electrode enhances the energy efficiency of the PBDBD reactors.

From this review, it is evident that the VOC removal efficiency of packed bed reactors is higher than of unpacked reactors. The presence of packing material in the reactor enhances the electric field in the area near the contact points between the pellets and homogeneously distributes the plasma in the reactor. The effect of various properties of packing materials such as dielectric constant, size, shape, surface properties (surface area, pore volume and pore size) on the discharge characteristics and abatement of different VOCs has been reviewed. The dielectric constant of the packing material is important in determining the discharge characteristics and decomposition efficiency of the PBDBD. The packing material with higher dielectric constant increases the decomposition efficiency of the reactor and the increase in decomposition efficiency saturates at particular dielectric constant of the packing material. The size of the packing material is chosen to maximize the contact points between the packing material without completely filling the reactor. Maximizing the contact points enhances the electric field and produces uniform plasma and the presence of gaps in the packing facilitates the generation of plasma. The hollow cylindrical shape of the packing material enhances the electric field due to the presence of sharp edges and thus increases the decomposition efficiency of the PBDBD reactor. The presence of a porous packing material increases the residence time of VOC in the discharge zone by adsorption and enhances the collisional probability between a VOC molecule and plasma generated active species. Porous material with higher surface area enhances the decomposition efficiency, increases CO₂ selectivity and results in complete oxidation of VOC. The pore size of the packing material is crucial for the adsorption of VOC as the porous material is efficient in adsorbing molecules smaller than its pore size. The porous packing material also enhances the discharge power due to the formation of additional microdischarges inside the pores. On the other hand, porous packing material shows deactivation with continuous usage due to the formation of coke deposit on the surface which blocks the pores. The activity of the packing material can be regenerated by oxygen plasma treatment.

Apart from enhancing the energy efficiency and decomposition efficiency, the presence of packing material significantly reduces the formation of unwanted by-products and enhances CO₂ selectivity. The presence of packing material reduces the formation of ozone due to decomposition of ozone on the surface of packing material. Packing the DBD reactor with porous packing material increases CO₂ selectivity and suppresses NO_x formation. On the other hand, the problem of formation of polymeric deposit due to continuous usage is still prevalent in the packed bed DBD reactor which results in poor carbon balances. The formation of polymeric deposit can be significantly reduced by presence of at least 1% O₂ in the feed gas and the solid carbon deposit can be removed using oxygen plasma.

The presence of a catalytic packing material produces active oxygen on the surface of the catalyst by the decomposition of ozone and this enhances the deep oxidation of VOCs and reduces the ozone concentration in the exhaust. The amount of metal loading on the packing material plays an important role in the formation of CO₂ by deep oxidation of organic intermediate products. The presence of metal catalysts in the packing material suppresses the formation of oxides of nitrogen which is one of the important toxic by-products produced in the presence of air in the feed gas.

Thus, the presence of packing material in the discharge region of the dielectric barrier discharge reactor enhances the energy efficiency, increases VOC removal efficiency, suppresses the formation of unwanted toxic by-products such as NO_x, ozone, other VOCs and significantly improves CO₂

selectivity when compared to the unpacked DBD reactor. On the other hand, for the commercialization of this technology, the lifetime of the porous packing material, deactivation of catalyst and the reaction kinetics for the different types of pollutants and catalysts in PBDBD reactors are important for this subject of research. An extensive investigation on the modification of the packing material and catalyst used in packed bed DBD reactors by the non-thermal plasma will be an important subject for this field of research.

Acknowledgments: This research has received funding from the Interreg 2014-2020 France-Wallonie-Vlaanderen program (EFRO) through the Depollutair project.

Author Contributions: Savita K. P. Veerapandian wrote the first draft of the article which was then refined by the comments and suggestions from Christophe Leys, Nathalie De Geyter and Rino Morent.

Conflicts of Interest: The authors declare no conflict of interest.

References

1. Nikolajsen, K.; Kiwi-Minsker, L.; Renken, A. Structured fixed-bed adsorber based on zeolite/sintered metal fibre for low concentration VOC removal. *Chem. Eng. Res. Des.* **2006**, *84*, 562–568. [[CrossRef](#)]
2. Ozturk, B.; Yilmaz, D. Absorptive removal of volatile organic compounds from flue gas streams. *Process Saf. Environ. Prot.* **2006**, *84*, 391–398. [[CrossRef](#)]
3. Poddar, T.K.; Majumdar, S.; Sirkar, K.K. Removal of VOCs from air by membrane-based absorption and stripping. *J. Memb. Sci.* **1996**, *120*, 221–237. [[CrossRef](#)]
4. Dwivedi, P.; Gaur, V.; Sharma, A.; Verma, N. Comparative study of removal of volatile organic compounds by cryogenic condensation and adsorption by activated carbon fiber. *Sep. Purif. Technol.* **2004**, *39*, 23–37. [[CrossRef](#)]
5. Gupta, V.K.; Verma, N. Removal of volatile organic compounds by cryogenic condensation followed by adsorption. *Chem. Eng. Sci.* **2002**, *57*, 2679–2696. [[CrossRef](#)]
6. Li, W.; Gong, H. Recent progress in the removal of volatile organic compounds by catalytic combustion. *Acta Phys. Chim. Sin.* **2010**, *26*, 885–894.
7. Qu, Z.; Bu, Y.; Qin, Y.; Wang, Y.; Fu, Q. The effects of alkali metal on structure of manganese oxide supported on SBA-15 for application in the toluene catalytic oxidation. *Chem. Eng. J.* **2012**, *209*, 163–169. [[CrossRef](#)]
8. Demeestere, K.; Dewulf, J.; Van Langenhove, H. Heterogeneous photocatalysis as an advanced oxidation process for the abatement of chlorinated, monocyclic aromatic and sulfurous volatile organic compounds in air: State of the art. *Crit. Rev. Environ. Sci. Technol.* **2007**, *37*, 489–538. [[CrossRef](#)]
9. Einaga, H.; Ibusuki, T.; Futamura, S. Photocatalytic oxidation of benzene in air. *J. Sol. Energy Eng.* **2004**, *126*, 789–793. [[CrossRef](#)]
10. Mo, J.; Zhang, Y.; Xu, Q.; Lamson, J.J.; Zhao, R. Photocatalytic purification of volatile organic compounds in indoor air: A literature review. *Atmos. Environ.* **2009**, *43*, 2229–2246. [[CrossRef](#)]
11. Kumar, A.; Dewulf, J.; Van Langenhove, H. Membrane-based biological waste gas treatment. *Chem. Eng. J.* **2008**, *136*, 82–91. [[CrossRef](#)]
12. Mudliar, S.; Giri, B.; Padoley, K.; Satpute, D.; Dixit, R.; Bhatt, P.; Pandey, R.; Juwarkar, A.; Vaidya, A. Bioreactors for treatment of VOCs and odours—A review. *J. Environ. Manag.* **2010**, *91*, 1039–1054. [[CrossRef](#)] [[PubMed](#)]
13. Wang, X.; Jia, X.; Wen, J. Transient modeling of toluene waste gas biotreatment in a gas-liquid airlift loop reactor. *Chem. Eng. J.* **2010**, *159*, 1–10. [[CrossRef](#)]
14. Khan, F.I.; Kr. Ghoshal, A. Removal of volatile organic compounds from polluted air. *J. Loss Prev. Process Ind.* **2000**, *13*, 527–545. [[CrossRef](#)]
15. Rani Parmar, G.; Rao, N.N. Emerging control technologies for volatile organic compounds. *Crit. Rev. Environ. Sci. Technol.* **2009**, *39*, 41–78. [[CrossRef](#)]
16. Luengas, A.; Barona, A.; Hort, C.; Gallastegui, G.; Platel, V.; Elias, A. A review of indoor air treatment technologies. *Rev. Environ. Sci. Biotechnol.* **2015**, *14*, 499–522. [[CrossRef](#)]
17. Hermia, J.; Vigneron, S. Catalytic incineration for odour abatement and VOC destruction. *Catal. Today* **1993**, *17*, 349–358. [[CrossRef](#)]

18. Zhu, X.; Gao, X.; Qin, R.; Zeng, Y.; Qu, R.; Zheng, C.; Tu, X. Plasma-catalytic removal of formaldehyde over Cu–Ce catalysts in a dielectric barrier discharge reactor. *Appl. Catal. B* **2015**, *170–171*, 293–300. [[CrossRef](#)]
19. Sivachandiran, L.; Karuppiyah, J.; Subrahmanyam, C. DBD plasma reactor for oxidative decomposition of chlorobenzene. *Int. J. Chem. React. Eng.* **2012**. [[CrossRef](#)]
20. Chen, H.L.; Lee, H.M.; Chen, S.H.; Chang, M.B.; Yu, S.J.; Li, S.N. Removal of volatile organic compounds by single-stage and two-stage plasma catalysis systems: A review of the performance enhancement mechanisms, current status, and suitable applications. *Environ. Sci. Technol.* **2009**, *43*, 2216–2227. [[CrossRef](#)] [[PubMed](#)]
21. Kim, H.-H. Nonthermal plasma processing for air-pollution control: A historical review, current issues, and future prospects. *Plasma Process. Polym.* **2004**, *1*, 91–110. [[CrossRef](#)]
22. Vandembroucke, A.M.; Morent, R.; De Geyter, N.; Leys, C. Non-thermal plasmas for non-catalytic and catalytic VOC abatement. *J. Hazard. Mater.* **2011**, *195*, 30–54. [[CrossRef](#)] [[PubMed](#)]
23. Oda, T. Non-thermal plasma processing for environmental protection: Decomposition of dilute VOCs in air. *J. Electrostat.* **2003**, *57*, 293–311. [[CrossRef](#)]
24. Van Durme, J.; Dewulf, J.; Leys, C.; Van Langenhove, H. Combining non-thermal plasma with heterogeneous catalysis in waste gas treatment: A review. *Appl. Catal. B* **2008**, *78*, 324–333. [[CrossRef](#)]
25. Trinh, Q.H.; Mok, Y.S. Effect of the adsorbent/catalyst preparation method and plasma reactor configuration on the removal of dilute ethylene from air stream. *Catal. Today* **2014**, *256*, 170–177. [[CrossRef](#)]
26. Li, S.; Tang, Z.C.; Gu, F. Experimental study on temperature characteristics and energy conversion in packed bed reactor with dielectric barrier discharge. *Heat Mass Transf.* **2010**, *46*, 851–857. [[CrossRef](#)]
27. Huang, L.; Nakajo, K.; Ozawa, S.; Matsuda, H. Decomposition of dichloromethane in a wire-in-tube pulsed corona reactor. *Environ. Sci. Technol.* **2001**, *35*, 1276–1281. [[CrossRef](#)] [[PubMed](#)]
28. Penetrante, B.M.; Hsiao, M.C.; Bardsley, J.N.; Merritt, B.T.; Vogtlin, G.E.; Kuthi, A.; Burkhart, C.P.; Bayless, J.R. Decomposition of methylene chloride by electron beam and pulsed corona processing. *Phys. Lett. A* **1997**, *235*, 76–82. [[CrossRef](#)]
29. Hsiao, M.C.; Merritt, B.T.; Penetrante, B.M.; Vogtlin, G.E.; Wallman, P.H. Plasma-assisted decomposition of methanol and trichloroethylene in atmospheric pressure air streams by electrical discharge processing. *J. Appl. Phys.* **1995**, *78*, 3451–3456. [[CrossRef](#)]
30. Penetrante, B.M.; Hsiao, M.C.; Bardsley, J.N.; Merritt, B.T.; Vogtlin, G.E.; Wallman, P.H.; Kuthi, A.; Burkhart, C.P.; Bayless, J.R. Electron beam and pulsed corona processing of carbon tetrachloride in atmospheric pressure gas streams. *Phys. Lett. A* **1995**, *209*, 69–77. [[CrossRef](#)]
31. Norberg, A. Modeling current pulse shape and energy in surface discharges. *IEEE Trans. Ind. Appl.* **1992**, *28*, 498–503. [[CrossRef](#)]
32. Rousseau, A.; Dantier, A.; Gatilova, L.; Ionikh, Y.; Röpcke, J.; Tolmachev, Y. On NO_x production and volatile organic compound removal in a pulsed microwave discharge in air. *Plasma Sources Sci. Technol.* **2005**, *14*, 70–75. [[CrossRef](#)]
33. Kogelschatz, U. Dielectric-barrier discharges: Their history, discharge physics, and industrial applications. *Plasma Chem. Plasma Process.* **2003**, *23*, 1–46. [[CrossRef](#)]
34. Evans, D.; Rosocha, L.A.; Anderson, G.K.; Coogan, J.J.; Kushner, M.J. Plasma remediation of trichloroethylene in silent discharge plasmas. *J. Appl. Phys.* **1993**, *74*, 5378–5386. [[CrossRef](#)]
35. Falkenstein, Z. Effects of the O₂ concentration on the removal efficiency of volatile organic compounds with dielectric barrier discharges in Ar and N₂. *J. Appl. Phys.* **1999**, *85*, 525–529. [[CrossRef](#)]
36. Snyder, H.R.; Anderson, G.K. Effect of air and oxygen content on the dielectric barrier discharge decomposition of chlorobenzene. *IEEE Trans. Plasma Sci.* **1998**, *26*, 1695–1699. [[CrossRef](#)]
37. Oda, T.; Takahashi, T.; Tada, K. Decomposition of dilute trichloroethylene by nonthermal plasma. *IEEE Trans. Ind. Appl.* **1999**, *35*, 373–379. [[CrossRef](#)]
38. Yamamoto, T.; Ramanathan, K.; Lawless, P.A.; Ensor, D.S.; Newsome, J.R.; Plaks, N.; Ramsey, G.H. Control of volatile organic compounds by an ac energized ferroelectric pellet reactor and a pulsed corona reactor. *IEEE Trans. Ind. Appl.* **1992**, *28*, 528–534. [[CrossRef](#)]
39. Tonkyn, R.G.; Barlow, S.E.; Orlando, T.M. Destruction of carbon tetrachloride in a dielectric barrier/packed-bed corona reactor. *J. Appl. Phys.* **1996**, *80*, 4877–4886. [[CrossRef](#)]
40. Yamamoto, T. Optimization of nonthermal plasma for the treatment of gas streams. *J. Hazard. Mater.* **1999**, *67*, 165–181. [[CrossRef](#)]

41. Kim, H.H.; Ogata, A.; Futamura, S. Effect of different catalysts on the decomposition of VOCs using flow-type plasma-driven catalysis. *IEEE Trans. Plasma Sci.* **2006**, *34*, 984–995. [[CrossRef](#)]
42. Ding, H.-X.; Zhu, A.-M.; Yang, X.-F.; Li, C.-H.; Xu, Y. Removal of formaldehyde from gas streams via packed-bed dielectric barrier discharge plasmas. *J. Phys. D* **2005**, *38*, 4160–4167. [[CrossRef](#)]
43. Liang, W.J.; Wang, A.; Ma, L.; Li, J. Combination of spontaneous polarization plasma and photocatalyst for toluene oxidation. *J. Electrostat.* **2015**, *75*, 27–34. [[CrossRef](#)]
44. Ogata, A.; Yamanouchi, K.; Mizuno, K.; Kushiyama, S.; Yamamoto, T. Oxidation of dilute benzene in an alumina hybrid plasma reactor at atmospheric pressure. *Plasma Chem. Plasma Process.* **1999**, *19*, 383–394. [[CrossRef](#)]
45. Chae, J.; Moon, S.; Sun, H.; Kim, K.; Vassiliev, V.A.; Mikhola, E.M. A study of volatile organic compounds decomposition with the use of non-thermal plasma. *KSME Int. J.* **1999**, *13*, 647–655. [[CrossRef](#)]
46. Ogata, A.; Ito, D.; Mizuno, K.; Kushiyama, S.; Gal, A.; Yamamoto, T. Effect of coexisting components on aromatic decomposition in a packed-bed plasma reactor. *Appl. Catal. A* **2002**, *236*, 9–15. [[CrossRef](#)]
47. Kim, H.H.; Kobara, H.; Ogata, A.; Futamura, S. Comparative assessment of different nonthermal plasma reactors on energy efficiency and aerosol formation from the decomposition of gas-phase benzene. *IEEE Trans. Ind. Appl.* **2005**, *41*, 206–214. [[CrossRef](#)]
48. Zhu, T.; Li, J.; Jin, Y.; Liang, Y.; Ma, G. Decomposition of benzene by non-thermal plasma processing: Photocatalyst and ozone effect. *Int. J. Environ. Sci. Technol.* **2008**, *5*, 375–384. [[CrossRef](#)]
49. Pangilinan, C.D.C.; Kurniawan, W.; Salim, C.; Hinode, H. Effect of Ag/TiO₂ catalyst preparation on gas-phase benzene decomposition using non-thermal plasma driven catalysis under oxygen plasma. *React. Kinet. Mech. Catal.* **2016**, *117*, 103–118. [[CrossRef](#)]
50. Li, J.; Han, S.; Bai, S.; Han, S.; Song, H.; Pu, Y.; Zhu, X.; Chen, W. Effect of Pt/gamma-Al₂O₃ catalyst on nonthermal plasma decomposition of benzene and byproducts. *Environ. Eng. Sci.* **2011**, *28*, 395–403. [[CrossRef](#)]
51. Fan, H.-Y.; Shi, C.; Li, X.-S.; Zhao, D.-Z.; Xu, Y.; Zhu, A.-M. High-efficiency plasma catalytic removal of dilute benzene from air. *J. Phys. D* **2009**, *42*, 225105. [[CrossRef](#)]
52. Kim, H.H.; Oh, S.M.; Ogata, A.; Futamura, S. Decomposition of benzene using Ag/TiO₂ packed plasma-driven catalyst reactor: Influence of electrode configuration and Ag-loading amount. *Catal. Lett.* **2004**, *96*, 189–194. [[CrossRef](#)]
53. Zhu, T.; Li, J.; Jin, Y.Q.; Liang, Y.H.; Ma, G.D. Gaseous phase benzene decomposition by non-thermal plasma coupled with nano titania catalyst. *Int. J. Environ. Sci. Technol.* **2009**, *6*, 141–148. [[CrossRef](#)]
54. Hu, J.; Jiang, N.; Li, J.; Shang, K.; Lu, N.; Wu, Y. Degradation of benzene by bipolar pulsed series surface/packed-bed discharge reactor over MnO₂-TiO₂/zeolite catalyst. *Chem. Eng. J.* **2016**, *293*, 216–224. [[CrossRef](#)]
55. Kim, H.H.; Lee, Y.H.; Ogata, A.; Futamura, S. Plasma-driven catalyst processing packed with photocatalyst for gas-phase benzene decomposition. *Catal. Commun.* **2003**, *4*, 347–351. [[CrossRef](#)]
56. Jiang, N.; Lu, N.; Li, J.; Wu, Y. Degradation of benzene by using a silent-packed bed hybrid discharge plasma reactor. *Plasma Sci. Technol.* **2012**, *14*, 140–146. [[CrossRef](#)]
57. Gandhi, M.S.; Mok, Y.S.; Lee, S.B.; Park, H. Effect of various parameters for butane decomposition under ambient temperature in a dielectric barrier discharge non-thermal plasma reactor. *J. Taiwan Inst. Chem. Eng.* **2013**, *44*, 786–794. [[CrossRef](#)]
58. Delagrangé, S.; Pinard, L.; Tatibout, J.M. Combination of a non-thermal plasma and a catalyst for toluene removal from air: Manganese based oxide catalysts. *Appl. Catal. B* **2006**, *68*, 92–98. [[CrossRef](#)]
59. Mok, Y.S.; Nam, C.M.; Cho, M.H.; Nam, I.S. Decomposition of volatile organic compounds and nitric oxide by nonthermal plasma discharge processes. *IEEE Trans. Plasma Sci.* **2002**, *30*, 408–416.
60. Lee, H.M.; Chang, M.B. Gas-phase removal of acetaldehyde via packed-bed dielectric barrier discharge reactor. *Plasma Chem. Plasma Process.* **2001**, *21*, 329–343. [[CrossRef](#)]
61. Liang, W.; Li, J.; Li, J.; Jin, Y. Abatement of toluene from gas streams via ferro-electric packed bed dielectric barrier discharge plasma. *J. Hazard. Mater.* **2009**, *170*, 633–638. [[CrossRef](#)] [[PubMed](#)]
62. Quoc An, H.T.; Pham Huu, T.; Le Van, T.; Cormier, J.M.; Khacef, A. Application of atmospheric non thermal plasma-catalysis hybrid system for air pollution control: Toluene removal. *Catal. Today* **2011**, *176*, 474–477. [[CrossRef](#)]

63. Dou, B.; Bin, F.; Wang, C.; Jia, Q.; Li, J. Discharge characteristics and abatement of volatile organic compounds using plasma reactor packed with ceramic Raschig rings. *J. Electrostat.* **2013**, *71*, 939–944. [[CrossRef](#)]
64. Takaki, K.; Hatanaka, Y.; Arima, K.; Mukaigawa, S.; Fujiwara, T. Influence of electrode configuration on ozone synthesis and microdischarge property in dielectric barrier discharge reactor. *Vacuum* **2008**, *83*, 128–132. [[CrossRef](#)]
65. Oda, T.; Yamaji, K.; Takahashi, T. Decomposition of dilute trichloroethylene by non-thermal plasma processing—frequency and catalyst effects. *IEEE Trans. Ind. Appl.* **2001**, *37*, 965–970. [[CrossRef](#)]
66. Ogata, A.; Miyamae, K.; Mizuno, K.; Kushiya, S.; Tezuka, M. Decomposition of benzene in air in a plasma reactor: Effect of reactor type and operating conditions. *Plasma Chem. Plasma Process.* **2002**, *22*, 537–552. [[CrossRef](#)]
67. Futamura, S.; Einaga, H.; Kabashima, H.; Hwan, L.Y. Synergistic effect of silent discharge plasma and catalysts on benzene decomposition. *Catal. Today* **2004**, *89*, 89–95. [[CrossRef](#)]
68. Wu, J.; Huang, Y.; Xia, Q.; Li, Z. Decomposition of toluene in a plasma catalysis system with NiO, MnO₂, CeO₂, Fe₂O₃, and CuO catalysts. *Plasma Chem. Plasma Process.* **2013**, *33*, 1073–1082. [[CrossRef](#)]
69. Kim, H.H.; Oh, S.M.; Ogata, A.; Futamura, S. Decomposition of gas-phase benzene using plasma-driven catalyst (PDC) reactor packed with Ag/TiO₂ catalyst. *Appl. Catal. B* **2005**, *56*, 213–220. [[CrossRef](#)]
70. Futamura, S.; Yamamoto, T.; Lawless, P.A. Towards understanding of VOC decomposition mechanisms using nonthermal plasmas. In Proceedings of the 1995 Thirtieth IAS Annual Meeting IEEE Conference Record of Industry Applications Conference, Orlando, FL, USA, 8–12 October 1995; Volume 2, pp. 1453–1458.
71. Yamamoto, T.; Mizuao, K.; Tamori, I.; Ogata, A.; Nifuku, M.; Michalska, M.; Prieto, G. Catalysis-assisted plasma technology for carbon tetrachloride destruction. *IEEE Trans. Ind. Appl.* **1996**, *32*, 100–105. [[CrossRef](#)]
72. Liang, W.J.; Li, J.; Li, J.X.; Zhu, T.; Jin, Y.Q. Formaldehyde removal from gas streams by means of NaNO₂ dielectric barrier discharge plasma. *J. Hazard. Mater.* **2010**, *175*, 1090–1095. [[CrossRef](#)] [[PubMed](#)]
73. He, C.; Cao, L.; Liu, X.; Fu, W.; Zhao, J. Catalytic behavior and synergistic effect of nonthermal plasma and CuO/AC catalyst for benzene destruction. *Int. J. Environ. Sci. Technol.* **2015**, *12*, 3531–3540. [[CrossRef](#)]
74. Ding, H.-X.; Zhu, A.-M.; Lu, F.-G.; Xu, Y.; Zhang, J.; Yang, X.-F. Low-temperature plasma-catalytic oxidation of formaldehyde in atmospheric pressure gas streams. *J. Phys. D* **2006**, *39*, 3603–3608. [[CrossRef](#)]
75. Chang, C.L.; Bai, H.; Lu, S.J. Destruction of styrene in an air stream by packed dielectric barrier discharge reactors. *Plasma Chem. Plasma Process.* **2005**, *25*, 641–657. [[CrossRef](#)]
76. Abd Allah, Z.; Sawtell, D.; Kasyutich, V.; Martin, P.A. FTIR and QCL diagnostics of the decomposition of volatile organic compounds in an atmospheric pressure dielectric packed bed plasma reactor. *J. Phys. Conf. Ser.* **2009**, *157*, 1–9. [[CrossRef](#)]
77. Fitzsimmons, C.; Ismail, F.; Whitehead, J.C.; Wilman, J.J. The chemistry of dichloromethane destruction in atmospheric-pressure gas streams by a dielectric packed-bed plasma reactor. *J. Phys. Chem. A* **2000**, *104*, 6032–6038. [[CrossRef](#)]
78. Okubo, M.; Yamamoto, T.; Kuroki, T.; Fukumoto, H. Electric air cleaner composed of nonthermal plasma reactor and electrostatic precipitator. *IEEE Trans. Ind. Appl.* **2001**, *37*, 1505–1511. [[CrossRef](#)]
79. Lin, C.-H.; Bai, H. Energy-effectiveness of nonthermal plasma reactors for toluene vapor destruction. *J. Environ. Eng.* **2001**, *127*, 648–654. [[CrossRef](#)]
80. Chang, C.L.; Lin, T.S. Decomposition of toluene and acetone in packed dielectric barrier discharge reactors. *Plasma Chem. Plasma Process.* **2005**, *25*, 227–243. [[CrossRef](#)]
81. Li, D.; Zhang, D.; Wu, Y.; Li, J.; Li, G. A study of removing chlorobenzene by the synergistic effect of catalysts and dielectric-barrier discharge Driven by bipolar pulse-power. *Plasma Sci. Technol.* **2008**, *10*, 94–99.
82. Okubo, M.; Kuroki, T.; Kametaka, H.; Yamamoto, T. Odor control using the ac barrier type plasma reactors. *IEEE Trans. Ind. Appl.* **2000**, 868–875.
83. Massines, F.; Gouda, G. A comparison of polypropylene-surface treatment by filamentary, homogeneous and glow discharges in helium at atmospheric pressure. *J. Phys. D* **1998**, *31*, 3411–3420. [[CrossRef](#)]
84. Manley, T.C. The electric characteristics of the ozonator discharge. *Trans. Electrochem. Soc.* **1943**, *84*, 83–96. [[CrossRef](#)]
85. Chirumamilla, V.R.; Hoeben, W.; Beckers, F.; Huiskamp, T.; Van Heesch, E.J.M.; Pemen, A.J.M. Experimental investigation on the effect of a microsecond pulse and a nanosecond pulse on NO removal using a pulsed DBD with catalytic materials. *Plasma Chem. Plasma Process.* **2016**, *36*, 487–510. [[CrossRef](#)]

86. Ogata, A.; Shintani, N.; Mizuno, K.; Kushiyama, S.; Yamamoto, T. Decomposition of benzene using a nonthermal plasma reactor packed with ferroelectric pellets. *IEEE Trans. Ind. Appl.* **1999**, *35*, 753–759. [[CrossRef](#)]
87. Tamaki, K.; Yoshida, H.; Katayama, T.; Kaido, C. Oxidation of nitrogen monoxide by corona discharges. 1. Effect of discharge conditions. *Nippon Kagaku Kaishi* **1979**, *11*, 1582–1588. [[CrossRef](#)]
88. Zheng, C.; Zhu, X.; Gao, X.; Liu, L.; Chang, Q.; Luo, Z.; Cen, K. Experimental study of acetone removal by packed-bed dielectric barrier discharge reactor. *J. Ind. Eng. Chem.* **2014**, *20*, 2761–2768. [[CrossRef](#)]
89. Chang, J.S.; Kostov, K.G.; Urashima, K.; Yamamoto, T.; Okayasu, Y.; Kato, T.; Iwaizumi, T.; Yoshimura, K. Removal of NF_3 from semiconductor process flue gases by tandem packed bed plasma-adsorbent hybrid systems. *IEEE Trans. Ind. Appl.* **1998**, *36*, 1845–1852.
90. Takaki, K.; Urashima, K.; Chang, J.S. Ferro-electric pellet shape effect on C_2F_6 removal by a packed-bed-type nonthermal plasma reactor. *IEEE Trans. Plasma Sci.* **2004**, *32*, 2175–2183. [[CrossRef](#)]
91. Jin, Q.; Jiang, B.; Han, J.; Yao, S. Hexane decomposition without particle emission using a novel dielectric barrier discharge reactor filled with porous dielectric balls. *Chem. Eng. J.* **2016**, *286*, 300–310. [[CrossRef](#)]
92. Urashima, K.; Kostov, K.G.; Chang, J.S.; Okayasu, Y.; Iwaizumi, T.; Yoshimura, K.; Kato, T. Removal of C_2F_6 from a semiconductor process flue gas by a ferroelectric packed-bed barrier discharge reactor with an adsorber. *IEEE Trans. Ind. Appl.* **2001**, *37*, 1456–1463. [[CrossRef](#)]
93. Tu, X.; Gallon, H.J.; Whitehead, J.C. Transition behavior of packed-bed dielectric barrier discharge in argon. *IEEE Trans. Plasma Sci.* **2011**, *39*, 2172–2173. [[CrossRef](#)]
94. Holzer, F.; Kopinke, F.D.; Roland, U. Influence of ferroelectric materials and catalysts on the performance of non-thermal plasma (NTP) for the removal of air pollutants. *Plasma Chem. Plasma Process.* **2005**, *25*, 595–611. [[CrossRef](#)]
95. Ogata, A.; Einaga, H.; Kabashima, H.; Futamura, S.; Kushiyama, S.; Kim, H.H. Effective combination of nonthermal plasma and catalysts for decomposition of benzene in air. *Appl. Catal. B* **2003**, *46*, 87–95. [[CrossRef](#)]
96. Oda, T.; Takahashi, T.; Yamaji, K. Nonthermal plasma processing for dilute VOCs decomposition. *IEEE Trans. Ind. Appl.* **2002**, *38*, 873–878. [[CrossRef](#)]
97. Chang, J.S.; Chakrabarti, A.; Urashima, K.; Arai, M. The effects of barium titanate pellet shapes on the gas discharge characteristics of ferroelectric packed bed reactors. In Proceedings of the 1998 Annual Report Conference on Electrical Insulation and Dielectric Phenomena, Atlanta, GA, USA, 25–28 October 1998; Volume 2, pp. 485–488.
98. Takaki, K.; Urashima, K.; Chang, J.S. Scale-up of ferro-electric packed bed reactor for C_2F_6 decomposition. *Thin Solid Films* **2006**, *506*, 414–417. [[CrossRef](#)]
99. Bradford, M.C.J.; Vannice, M.A. Estimation of CO heats of adsorption on metal surfaces from vibrational spectra. *Ind. Eng. Chem. Res.* **1996**, *35*, 3171–3178. [[CrossRef](#)]
100. Lee, B.Y.; Park, S.H.; Lee, S.C.; Kang, M.; Choung, S.J. Decomposition of benzene by using a discharge plasma-photocatalyst hybrid system. *Catal. Today* **2004**, *93–95*, 769–776. [[CrossRef](#)]
101. Takahashi, A.; Yang, F.H.; Yang, R.T. Aromatics/aliphatics separation by adsorption: New sorbents for selective aromatics adsorption by π -complexation. *Ind. Eng. Chem. Res.* **2000**, *39*, 3856–3867. [[CrossRef](#)]
102. Gandhi, M.S.; Ananth, A.; Mok, Y.S.; Song, J.I.; Park, K.H. Effect of porosity of α -alumina on non-thermal plasma decomposition of ethylene in a dielectric-packed bed reactor. *Res. Chem. Intermed.* **2014**, *40*, 1483–1493. [[CrossRef](#)]
103. Holzer, F.; Roland, U.; Kopinke, F.D. Combination of non-thermal plasma and heterogeneous catalysis for oxidation of volatile organic compounds. Part 1. Accessibility of the intra-particle volume. *Appl. Catal. B* **2002**, *38*, 163–181. [[CrossRef](#)]
104. Ogata, A.; Ito, D.; Mizuno, K.; Kushiyama, S.; Yamamoto, T. Removal of dilute benzene using a zeolite-hybrid plasma reactor. *IEEE Trans. Ind. Appl.* **2001**, *37*, 959–964. [[CrossRef](#)]
105. Zhu, R.; Mao, Y.; Jiang, L.; Chen, J. Performance of chlorobenzene removal in a nonthermal plasma catalysis reactor and evaluation of its byproducts. *Chem. Eng. J.* **2015**, *279*, 463–471. [[CrossRef](#)]
106. Dey, G.R.; Sharma, A.; Pushpa, K.K.; Das, T.N. Variable products in dielectric-barrier discharge assisted benzene oxidation. *J. Hazard. Mater.* **2010**, *178*, 693–698. [[CrossRef](#)] [[PubMed](#)]

107. Gandhi, M.S.; Ananth, A.; Mok, Y.S.; Song, J.I.; Park, K.H. Time dependence of ethylene decomposition and byproducts formation in a continuous flow dielectric-packed plasma reactor. *Chemosphere* **2013**, *91*, 685–691. [[CrossRef](#)] [[PubMed](#)]
108. Ogata, A.; Shintani, N.; Yamanouchi, K.; Mizuno, K.; Kushiyama, S.; Yamamoto, T. Effect of water vapor on benzene decomposition using a nonthermal-discharge plasma reactor. *Plasma Chem. Plasma Process.* **2000**, *20*, 453–467. [[CrossRef](#)]
109. Zhao, D.-Z.; Li, X.-S.; Shi, C.; Fan, H.-Y.; Zhu, A.-M. Low-concentration formaldehyde removal from air using a cycled storage-discharge (CSD) plasma catalytic process. *Chem. Eng. Sci.* **2011**, *66*, 3922–3929. [[CrossRef](#)]
110. Huang, H.; Ye, D.; Leung, D.Y.C. Abatement of toluene in the plasma-driven catalysis: Mechanism and reaction kinetics. *IEEE Trans. Plasma Sci.* **2011**, *39*, 877–882. [[CrossRef](#)]
111. Ogata, A.; Yamanouchi, K.; Mizuno, K.; Kushiyama, S.; Yamamoto, T. Decomposition of benzene using alumina-hybrid and catalyst-hybrid plasma reactors. *IEEE Trans. Ind. Appl.* **1999**, *35*, 1289–1295. [[CrossRef](#)]
112. Trinh, H.Q.; Mok, Y.S. Plasma-catalytic oxidation of acetone in annular porous monolithic ceramic-supported catalysts. *Chem. Eng. J.* **2014**, *251*, 199–206. [[CrossRef](#)]
113. Horvath, G.; Mason, N.J.; Polachova, L.; Zahoran, M.; Moravsky, L.; Matejcek, S. Packed bed DBD discharge experiments in admixtures of N₂ and CH₄. *Plasma Chem. Plasma Process.* **2010**, *30*, 565–577. [[CrossRef](#)]
114. Futamura, S.; Zhang, A.; Einaga, H.; Kabashima, H. Involvement of catalyst materials in nonthermal plasma chemical processing of hazardous air pollutants. *Catal. Today* **2002**, *72*, 259–265. [[CrossRef](#)]
115. Futamura, S.; Zhang, A.; Yamamoto, T. Mechanisms for formation of inorganic byproducts in plasma chemical processing of hazardous air pollutants. *IEEE Trans. Ind. Appl.* **1999**, *35*, 760–766. [[CrossRef](#)]
116. Lu, M.; Huang, R.; Wu, J.; Fu, M.; Chen, L.; Ye, D. On the performance and mechanisms of toluene removal by FeO_x/SBA-15-assisted non-thermal plasma at atmospheric pressure and room temperature. *Catal. Today* **2015**, *242*, 274–286. [[CrossRef](#)]
117. Zhu, X.; Gao, X.; Yu, X.; Zheng, C.; Tu, X. Catalyst screening for acetone removal in a single-stage plasma-catalysis system. *Catal. Today* **2014**, *256*, 108–114. [[CrossRef](#)]
118. Zhu, X.; Tu, X.; Mei, D.; Zheng, C.; Zhou, J.; Gao, X.; Luo, Z.; Ni, M.; Cen, K. Investigation of hybrid plasma-catalytic removal of acetone over CuO/γ-Al₂O₃ catalysts using response surface method. *Chemosphere* **2016**, *155*, 9–17. [[CrossRef](#)] [[PubMed](#)]
119. Oda, T.; Takahashi, T.; Yamaji, K. TCE decomposition by the nonthermal plasma process concerning ozone effect. *IEEE Trans. Ind. Appl.* **2004**, *40*, 1249–1256. [[CrossRef](#)]
120. Harling, A.M.; Demidyuk, V.; Fischer, S.J.; Whitehead, J.C. Plasma-catalysis destruction of aromatics for environmental clean-up: Effect of temperature and configuration. *Appl. Catal. B* **2008**, *82*, 180–189. [[CrossRef](#)]
121. Oda, T.; Yamaji, K.; Takahashi, T. Decomposition of dilute trichloroethylene by nonthermal plasma processing—Gas flow rate, catalyst, and ozone effect. *IEEE Trans. Ind. Appl.* **2004**, *40*, 430–436. [[CrossRef](#)]
122. Jiang, L.; Nie, G.; Zhu, R.; Wang, J.; Chen, J.; Mao, Y.; Cheng, Z.; Anderson, W.A. Efficient degradation of chlorobenzene in a non-thermal plasma catalytic reactor supported on CeO₂/HZSM-5 catalysts. *J. Environ. Sci.* **2016**, 1–8. [[CrossRef](#)] [[PubMed](#)]
123. Wang, L.; Huang, B.; Su, Y.; Zhou, G.; Wang, K.; Luo, H.; Ye, D. Manganese oxides supported on multi-walled carbon nanotubes for selective catalytic reduction of NO with NH₃: Catalytic activity and characterization. *Chem. Eng. J.* **2012**, *192*, 232–241. [[CrossRef](#)]
124. Li, H.; Lu, G.; Dai, Q.; Wang, Y.; Guo, Y.; Guo, Y. Efficient low-temperature catalytic combustion of trichloroethylene over flower-like mesoporous Mn-doped CeO₂ microspheres. *Appl. Catal. B* **2011**, *102*, 475–483. [[CrossRef](#)]
125. Ogata, A.; Kim, H.H.; Futamura, S.; Kushiyama, S.; Mizuno, K. Effects of catalysts and additives on fluorocarbon removal with surface discharge plasma. *Appl. Catal. B* **2004**, *53*, 175–180. [[CrossRef](#)]
126. Kim, H.H.; Ogata, A.; Schiorlin, M.; Marotta, E.; Paradisi, C. Oxygen isotope (18O₂) evidence on the role of oxygen in the plasma-driven catalysis of VOC oxidation. *Catal. Lett.* **2011**, *141*, 277–282. [[CrossRef](#)]
127. Kang, M.; Kim, B.J.; Cho, S.M.; Chung, C.H.; Kim, B.W.; Han, G.Y.; Yoon, K.J. Decomposition of toluene using an atmospheric pressure plasma/TiO₂ catalytic system. *J. Mol. Catal. A* **2002**, *180*, 125–132. [[CrossRef](#)]
128. Zhu, T.; Li, J.; Liang, W.; Jin, Y. Synergistic effect of catalyst for oxidation removal of toluene. *J. Hazard. Mater.* **2009**, *165*, 1258–1260. [[CrossRef](#)] [[PubMed](#)]
129. Bahri, M.; Haghghat, F.; Rohani, S.; Kazemian, H. Impact of design parameters on the performance of non-thermal plasma air purification system. *Chem. Eng. J.* **2016**, *302*, 204–212. [[CrossRef](#)]

130. Fan, X.; Zhu, T.; Wan, Y.; Yan, X. Effects of humidity on the plasma-catalytic removal of low-concentration BTX in air. *J. Hazard. Mater.* **2010**, *180*, 616–621. [[CrossRef](#)] [[PubMed](#)]
131. Ran, L.; Wang, Z.; Wang, X. The effect of Ce on catalytic decomposition of chlorinated methane over RuO_x catalysts. *Appl. Catal. A* **2014**, *470*, 442–450. [[CrossRef](#)]
132. Lee, H.; Lee, D.H.; Song, Y.H.; Choi, W.C.; Park, Y.K.; Kim, D.H. Synergistic effect of non-thermal plasma-catalysis hybrid system on methane complete oxidation over Pd-based catalysts. *Chem. Eng. J.* **2015**, *259*, 761–770. [[CrossRef](#)]
133. Chen, L.; Zhang, X.; Huang, L.; Lei, L. Application of in-plasma catalysis and post-plasma catalysis for methane partial oxidation to methanol over a Fe₂O₃-CuO/γ-Al₂O₃ catalyst. *J. Nat. Gas Chem.* **2010**, *19*, 628–637. [[CrossRef](#)]
134. Aerts, R.; Tu, X.; Van Gaens, W.; Whitehead, J.C.; Bogaerts, A. Gas purification by nonthermal plasma: A case study of ethylene. *Environ. Sci. Technol.* **2013**, *47*, 6478–6485. [[PubMed](#)]
135. Burg, S.P.; Burg, E.A. Role of ethylene in fruit ripening. *Plant Physiol.* **1962**, *37*, 179–189. [[CrossRef](#)] [[PubMed](#)]
136. Harling, A.M.; Glover, D.J.; Whitehead, J.C.; Zhang, K. Novel method for enhancing the destruction of environmental pollutants by the combination of multiple plasma discharges. *Environ. Sci. Technol.* **2008**, *42*, 4546–4550. [[CrossRef](#)] [[PubMed](#)]
137. Li, J.; Ma, C.; Xu, X.; Yu, J.; Hao, Z.; Qiao, S. Efficient elimination of trace ethylene over nano-gold catalyst under ambient conditions. *Environ. Sci. Technol.* **2008**, *42*, 8947–8951. [[CrossRef](#)] [[PubMed](#)]
138. Jiang, N.; Li, J.; Shang, K.; Lu, N.; Wu, Y. Enhanced degradation of benzene in surface/packed-bed hybrid discharge system: Optimization of the reactor structure and electrical parameters. *IEEE Trans. Plasma Sci.* **2016**, *44*, 657–664. [[CrossRef](#)]
139. Guerra, G.; Lemma, A.; Lerda, D.; Martines, C.; Salvi, G.; Tamponi, M. Benzene emissions from motor vehicle traffic in the urban area of milan: Hypothesis of health impact assessment. *Atmos. Environ.* **1995**, *29*, 3559–3569. [[CrossRef](#)]
140. Jones, A.P. Indoor air quality and health. *Atmos. Environ.* **1999**, *33*, 4535–4564. [[CrossRef](#)]
141. Coates, J.D.; Chakraborty, R.; Lack, J.G.; O'Connor, S.M.; Cole, K.A.; Bender, K.S.; Achenbach, L.A. Anaerobic benzene oxidation coupled to nitrate reduction in pure culture by two strains of *Dechloromonas*. *Nature* **2001**, *411*, 1039–1043. [[CrossRef](#)] [[PubMed](#)]
142. Futamura, S.; Gurusamy, A. Synergy of nonthermal plasma and catalysts in the decomposition of fluorinated hydrocarbons. *J. Electrostat.* **2005**, *63*, 949–954. [[CrossRef](#)]
143. Huang, H.B.; Ye, D.Q.; Fu, M.L.; Feng, F. Da Contribution of UV light to the decomposition of toluene in dielectric barrier discharge plasma/photocatalysis system. *Plasma Chem. Plasma Process.* **2007**, *27*, 577–588. [[CrossRef](#)]
144. Zhu, T.; Wan, Y.D.; Li, J.; He, X.W.; Xu, D.Y.; Shu, X.Q.; Liang, W.J.; Jin, Y.Q. Volatile organic compounds decomposition using nonthermal plasma coupled with a combination of catalysts. *Int. J. Environ. Sci. Technol.* **2011**, *8*, 621–630. [[CrossRef](#)]
145. Gibbs, B.F.; Mulligan, C.N. Styrene toxicity: An ecotoxicological assessment. *Ecotoxicol. Environ. Saf.* **1997**, *38*, 181–194. [[CrossRef](#)] [[PubMed](#)]
146. Kuroki, T.; Hirai, K.; Kawabata, R.; Okubo, M.; Yamamoto, T. Decomposition of adsorbed xylene on adsorbents using nonthermal plasma with gas circulation. *IEEE Trans. Ind. Appl.* **2010**, *46*, 672–679. [[CrossRef](#)]
147. Carpenter, C.P.; Geary, D.L.; Myers, R.C.; Nachreiner, D.J.; Sullivan, L.J.; King, J.M. Petroleum hydrocarbon toxicity studies XVII. Animal response to *n*-nonane vapor. *Toxicol. Appl. Pharmacol.* **1978**, *44*, 53–61. [[CrossRef](#)]
148. Nilsen, O.G.; Haugen, O.A.; Zahlsten, K.; Halgunset, J.; Helseth, A.; Aarset, H.; Eide, I. Toxicity of *n*-C₉ to *n*-C₁₃ alkanes in the rat on short term inhalation. *Pharmacol. Toxicol.* **1988**, *62*, 259–266. [[CrossRef](#)] [[PubMed](#)]
149. Niaz, K.; Bahadar, H.; Maqbool, F.; Abdollahi, M. A review of environmental and occupational exposure to xylene and its health concerns. *EXCLI J.* **2015**, *14*, 1167–1186. [[PubMed](#)]
150. Saulich, K.; Müller, S. Removal of formaldehyde by adsorption and plasma treatment of mineral adsorbent. *J. Phys. D* **2013**, *46*, 45201. [[CrossRef](#)]
151. US Environmental protection agency (EPA) (Office if Air and Radiation). *Introduction to Indoor Quality, a Reference Manual*; EPA: Washington, DC, USA, 1991; Volume EPA/400/3.

152. National Research Council of the National Academics (US). *Review of the Environmental Protection Agency's Draft IRIS Assessment of Formaldehyde*; National Research Council of the National Academics: Washington, DC, USA, 2011.
153. Barker, J.R.; Herstrom, A.A.; Tingey, D.T. Formaldehyde: Environmental partitioning and vegetation exposed. *Water Air Soil Pollut.* **1996**, *86*, 71–91. [[CrossRef](#)]
154. Flowers, L.; Broder, M.W.; Forsyth, C. *Toxicological Review of Acetone*; Environmental Protection Agency: Washington, DC, USA, 2003.
155. Urashima, K.; Chang, J.S. Removal of volatile organic compounds from air streams and industrial flue gases by non-thermal plasma technology. *IEEE Trans. Dielectr. Electr. Insul.* **2000**, *7*, 602–614. [[CrossRef](#)]
156. Zhang, A.; Futamura, S.; Yamamoto, T. Nonthermal plasma chemical processing of bromomethane. *J. Air Waste Manag. Assoc.* **1999**, *49*, 1442–1448. [[CrossRef](#)] [[PubMed](#)]
157. Langård, S.; Rognum, T.; Fløtterød, Ø.; Skaug, V. Fatal accident resulting from methyl bromide poisoning after fumigation of a neighbouring house leakage through sewage pipes. *J. Appl. Toxicol.* **1996**, *16*, 445–448. [[CrossRef](#)]
158. Bolt, H.M.; Gansewendt, B. Mechanisms of carcinogenicity of methyl halides. *Crit. Rev. Toxicol.* **1993**, *23*, 237–253. [[CrossRef](#)] [[PubMed](#)]
159. Ames, B.N.; Gold, L.S. Animal cancer tests and cancer prevention. *J. Natl. Cancer Inst. Monogr.* **1992**, 125–132.
160. Basu, S. Carbon tetrachloride-induced lipid peroxidation: Eicosanoid formation and their regulation by antioxidant nutrients. *Toxicology* **2003**, *189*, 113–127. [[CrossRef](#)]
161. Howards, P. *Handbook of Environmental Fate and Exposure Data for Organic Chemicals*; Lewis Publishers: Chelsea, MI, USA, 1989; Volume 2.
162. Harling, A.M.; Wallis, A.E.; Whitehead, J.C. The effect of temperature on the removal of DCM using non-thermal, atmospheric-pressure plasma-assisted catalysis. *Plasma Process. Polym.* **2007**, *4*, 463–470. [[CrossRef](#)]
163. Abd Allah, Z.; Whitehead, J.C.; Martin, P. Remediation of dichloromethane (CH₂Cl₂) using non-thermal, atmospheric pressure plasma generated in a packed-bed reactor. *Environ. Sci. Technol.* **2014**, *48*, 558–565. [[CrossRef](#)] [[PubMed](#)]
164. Bell, B.P.; Franks, P.; Hildreth, N.; Melius, J. Methylene chloride exposure and birthweight in Monroe County, New York. *Environ. Res.* **1991**, *55*, 31–39. [[CrossRef](#)]
165. Abedi, K.; Ghorbani-Shahna, F.; Jaleh, B.; Bahrami, A.; Yarahmadi, R.; Haddadi, R.; Gandomi, M. Decomposition of chlorinated volatile organic compounds (CVOCs) using NTP coupled with TiO₂/GAC, ZnO/GAC, and TiO₂-ZnO/GAC in a plasma-assisted catalysis system. *J. Electrostat.* **2015**, *73*, 80–88. [[CrossRef](#)]
166. Karuppiyah, J.; Reddy, P.M.K.; Reddy, L.E.; Subrahmanyam, C. Catalytic non-thermal plasma reactor for decomposition of dilute chlorobenzene. *Plasma Process. Polym.* **2013**, *10*, 1074–1080. [[CrossRef](#)]
167. Wang, C.; Xi, J.Y.; Hu, H.Y.; Yao, Y. Advantages of combined UV photodegradation and biofiltration processes to treat gaseous chlorobenzene. *J. Hazard. Mater.* **2009**, *171*, 1120–1125. [[CrossRef](#)] [[PubMed](#)]
168. Ogata, A.; Mizuno, K. Methane decomposition in a barium titanate packed-bed nonthermal plasma reactor. *Plasma Chem. Plasma Process.* **1998**, *18*, 363–373. [[CrossRef](#)]
169. Futamura, S.; Zhang, A.; Prieto, G.; Yamamoto, T. Factors and intermediates governing byproduct distribution for decomposition of butane in nonthermal plasma. *IEEE Trans. Ind. Appl.* **1998**, *34*, 967–974. [[CrossRef](#)]
170. Zhang, H.; Li, K.; Sun, T.; Jia, J.; Lou, Z.; Feng, L. Removal of styrene using dielectric barrier discharge plasmas combined with sol-gel prepared TiO₂ coated γ -Al₂O₃. *Chem. Eng. J.* **2014**, *241*, 92–102. [[CrossRef](#)]
171. Zhang, L.; Yang, D.; Wang, W.; Wang, S.; Yuan, H.; Zhao, Z.; Sang, C.; Jia, L. Needle-array to plate DBD plasma using sine AC and nanosecond pulse excitations for purpose of improving indoor air quality. *Sci. Rep.* **2016**, *6*, 25242. [[CrossRef](#)] [[PubMed](#)]
172. Wallis, A.E.; Whitehead, J.C.; Zhang, K. The removal of dichloromethane from atmospheric pressure nitrogen gas streams using plasma-assisted catalysis. *Appl. Catal. B* **2007**, *74*, 111–116. [[CrossRef](#)]

